iScience

CellPress
OPEN ACCESS

Article

A photoswitchable helical peptide with light-controllable interface/transmembrane topology in lipidic membranes

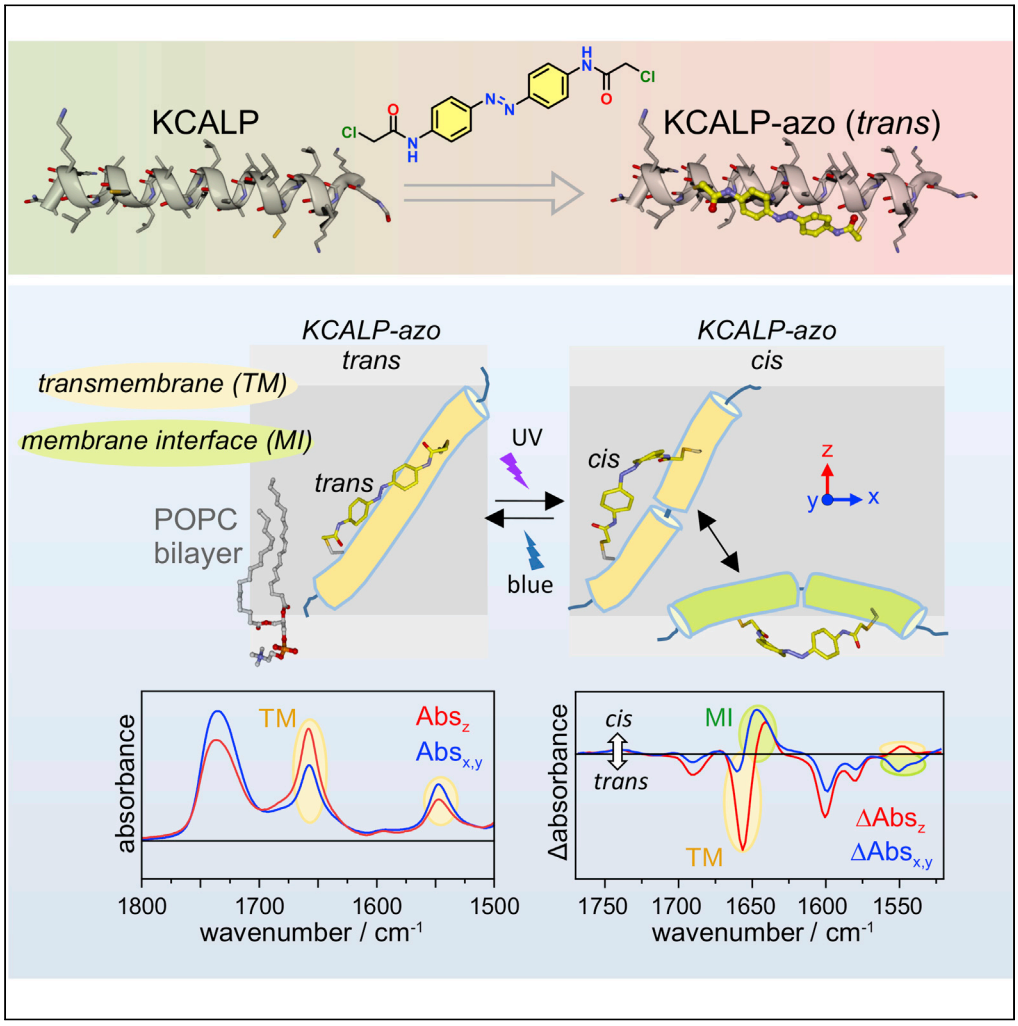

Mónica Gutiérrez-Salazar, Eduardo Santamaría-Aranda, Louise Schaar, Jesús Salgado, Diego Sampedro, Victor A. Lorenz-Fonfria

victor.lorenz@uv.es

Highlights

We present an α-helical transmembrane peptide modified with a molecular photoswitch

The peptide exhibits reversible photocontrol of its membrane topology

A fraction moves to the membrane interface with UV and inserts back with blue light

This system will be useful to address the molecular mechanism for membrane insertion

Gutiérrez-Salazar et al., iScience 24, 102771
July 23, 2021
https://doi.org/10.1016/j.isci.2021.102771

iScience

CellPress
OPEN ACCESS

Article

A photoswitchable helical peptide with light-controllable interface/transmembrane topology in lipidic membranes

Mónica Gutiérrez-Salazar,[1,3] Eduardo Santamaría-Aranda,[2,3] Louise Schaar,[1,4] Jesús Salgado,[1] Diego Sampedro,[2] and Victor A. Lorenz-Fonfria[1,5,*]

SUMMARY

The spontaneous insertion of helical transmembrane (TM) polypeptides into lipid bilayers is driven by three sequential equilibria: solution-to-membrane interface (MI) partition, unstructured-to-helical folding, and MI-to-TM helix insertion. A bottleneck for understanding these three steps is the lack of experimental approaches to perturb membrane-bound hydrophobic polypeptides out of equilibrium rapidly and reversibly. Here, we report on a 24-residues-long hydrophobic α-helical polypeptide, covalently coupled to an azobenzene photoswitch (KCALP-azo), which displays a light-controllable TM/MI equilibrium in hydrated lipid bilayers. FTIR spectroscopy reveals that *trans* KCALP-azo folds as a TM α-helix (TM topology). After *trans*-to-*cis* photoisomerization of the azobenzene moiety with UV light (reversed with blue light), the helical structure of KCALP-azo is maintained, but its helix tilt increased from 32 ± 5° to 79 ± 8°, indication of a reversible TM-to-MI transition. Further analysis indicates that this transition is incomplete, with *cis* KCALP-azo existing in a ~90% TM and ~10% MI mixture.

INTRODUCTION

Transmembrane (TM) α-helical proteins are involved in energy transduction and in the regulation of the traffic of molecules and information across biological membranes, processes of high biological relevance. In the cellular context, the insertion of TM segments of membrane proteins is in most cases assisted by a specialized protein complex called the translocon and carried out almost synchronously with polypeptide synthesis by the ribosome (Park and Rapoport, 2012). Nevertheless, mildly hydrophobic TM domains of C-terminally anchored proteins can insert spontaneously into membranes, without translocon participation (Brambillasca et al., 2006). Amphiphilic polypeptides, with antimicrobial, antitumoral, or apoptotic effects (Guha et al., 2019), provide another relevant example for the spontaneous membrane insertion of TM α-helices.

The well-established *three-step* model popularized by White et al. postulates that the spontaneous folding of TM helical protein fragments and peptides into lipid bilayers involves a solution-to-membrane interface (MI) partition, followed by folding into a helical structure, and completed by an MI-to-TM transition (White and Wimley, 1999). This sequence of events has been broadly supported by experimental data (White and Wimley, 1999) and molecular dynamics simulations (Ulmschneider and Ulmschneider, 2018). However, experimental details on the partition, folding, and insertion mechanisms, and their associated dynamics in both their forward and backward directions, remain poorly characterized. One reason for that stems from difficulties in perturbing TM helices out of their equilibrium. Hydrophobic peptides that form TM helices, although ideal models of membrane protein fragments, typically aggregate when added to aqueous solutions. Additionally, once inserted in membranes, they are very stable and unlikely to move back to the interface of the membrane, or to unfold.

One approach to experimentally study the insertion of peptides in lipidic membranes has been the use of pH-sensitive peptides, such as pHLIP, which exists in a water-soluble/MI equilibrium at neutral pH but inserts as a TM helix by decreasing the pH (Hunt et al., 1997). This property was exploited to externally induce the binding, folding, and TM insertion of pHLIP *via* rapid changes in the medium pH by stopped-flow (Andreev et al., 2010; Tang and Gai, 2008). However, the observed changes have been limited to a resolution of milliseconds and to single wavelength traces from Trp fluorescence spectroscopy, with limited information

[1]Institute of Molecular Science, Universitat de València, 46980 Paterna, Spain

[2]Departamento de Química, Universidad de la Rioja, Centro de investigación en Síntesis Química, Madre de Dios 53, 26006 Logroño, Spain

[3]These authors contributed equally

[4]Present address: Faculty of Natural Sciences from the Leibniz University of Hannover, Germany

[5]Lead contact

*Correspondence: victor.lorenz@uv.es

https://doi.org/10.1016/j.isci.2021.102771

content. An alternative approach has been to induce the TM insertion of a membrane-bound peptide by rapidly increasing the membrane fluidity with a laser-induced temperature-jump (T-jump) (Schuler et al., 2016). Although this allowed for (sub)microsecond resolution and sample conditions compatible with infrared (IR) spectroscopy, the changes in the membrane fluidity lasted for less than 1 ms (Schuler et al., 2016), making relevant millisecond and slower dynamical events inaccessible.

Some of the limitations of fast mixing methods (Roder et al., 2006) and T-jumps (Kubelka, 2009) for the folding/unfolding of water-soluble peptides have been avoided by their coupling to photoisomerizable organic molecules known as photoswitches (Blanco-Lomas et al., 2012; Hamm et al., 2008; Kumita et al., 2000). Most commonly, cysteine-reactive azobenzene derivatives have been linked to helical peptides, using as an anchor the thiol side chains of two cysteines (Flint et al., 2002). Changes in the azobenzene end-to-end length as it photoisomerizes from *trans* to *cis*, typically from ~18 Å to ~10 Å, are used to distort/unfold the structure of the coupled helical peptide with light (Flint et al., 2002; Woolley, 2005). The *trans* isomer can be restored upon exposure to light of a different wavelength, or thermally (Kumita et al., 2000). By this approach, the folding/unfolding of helical soluble peptides has been studied by time-resolved IR difference spectroscopy (Bredenbeck et al., 2005; Hamm et al., 2008; Ihalainen et al., 2007). In addition, the coupling of photoswitches to soluble peptides has also been used to control their interaction with proteins or with DNA/RNA (Albert and Vázquez, 2019; Beharry and Woolley, 2011). In other cases, proteins themselves have been modified with photoswitches, allowing a direct optical control of their activity (Hoersch et al., 2013; Mutter et al., 2019; Szymański et al., 2013). In addition, photoswitches have been inserted in the molecular skeleton of many ligand compounds that are able to activate or inhibit proteins, making their affinity to target proteins light-sensitive, key for the development of the field of photopharmacology (Hoorens and Szymanski, 2018).

Photoswitches have been used as well to control the structure and activity of amphiphilic peptides (Kim et al., 2018; Kneissl et al., 2008; Lee et al., 2020). These peptides typically display membrane permeabilizing properties related to antimicrobial, antitumoral or apoptotic activities (Guha et al., 2019). They are water-soluble peptides that form hydrophobic and hydrophilic surfaces when adopting a helical structure, a condition that favors their binding to the surface of membranes. In spite of their membrane interaction, amphiphilic peptides might not be ideal models to study the insertion and folding of helical TM fragments. Briefly, they might induce the formation of lipidic toroidal pores and adopt a TM topology without strictly inserting in membranes (Fuertes et al., 2011), and even when they do insert, they might adopt poorly defined heterogeneous helical oligomers (Ulmschneider and Ulmschneider, 2018). Besides amphiphilic peptides, there are also recent examples of the integration of photoswitches into membrane-interacting cyclic β-hairpin peptides, derived from gramicidin S, with the goal of tuning their antimicrobial activity with light (Babii et al, 2014, 2018; Yeoh et al., 2018).

Despite the proven utility of photoswitches, the potential of using them on hydrophobic α-helical peptides remains unexplored. In this work, we synthesized the photoswitchable peptide KCALP-azo, derived from the KALP family of peptides, used in the past as models for monomeric TM α-helices, both in experiments and simulations (Strandberg et al., 2012; Ulmschneider et al., 2010; Zhang et al., 1995). By means of FTIR absorption and difference spectroscopy, we concluded that KCALP-azo folds in lipidic membranes as a TM α-helix in the dark (*trans* azobenzene conformation). Upon *trans*-to-*cis* azobenzene isomerization, induced with UV light, a fraction of KCALP-azo reorients to lay almost parallel to the membrane surface. This drastic change of the helix tilt, accompanied by an increase of the polarity sensed by the peptide backbone, informs about a change in the membrane topology of KCALP-azo from a TM to an MI state. This change was reversed by restoring the *trans* conformation of azobenzene with blue light illumination, demonstrating for the first time to our knowledge, the reversible and specific manipulation of the TM/MI equilibrium of a hydrophobic peptide with light.

RESULTS

We constructed a 24 residues-long hydrophobic peptide with cysteine residues at positions 7 and 18 (*i*, *i*+11) and sequence Ac-GKKLLACLLAALLAALLCALLKKA-NH_2 (Figure 1A), hereafter KCALP, as well as a control version with the two Cys exchanged to Ala, hereafter KALP. Then, we incorporated the thiol-reactive cross-linker 4,4′-bis(chloroacetamide)azobenzene (BCA in Figure 1C, left) to KCALP, *via* cysteine side chains, adapting a protocol initially proposed to modify helical soluble peptides (Pozhidaeva et al., 2004), giving the photoswitchable peptide KCALP-azo (Figure 1B). As a spectroscopic control, we synthesized an azobenzene derivative that chemically mimics the product of the reaction of BCA with two thiol chains, named for short ThioAzo (Figure 1C, right).

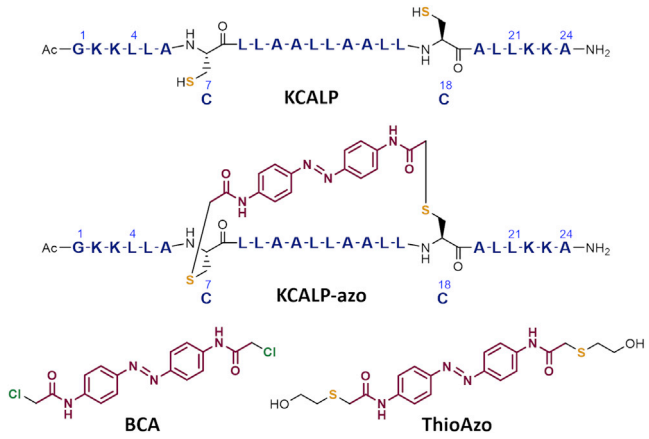

Figure 1. Structural comparison of KCALP, KCALP-azo, BCA, and ThioAzo

(A) Primary structure of the peptide KCALP, with the chemical structure of Cys7 and Cys18 (C7 and C18).

(B) Primary structure of the photoswitchable peptide KCALP-azo, with the chemical structure for Cys residues and for the azobenzene group.

(C) Chemical structure of the cysteine-reactive azobenzene-based cross-linker BCA (left), and of the compound ThioAzo (right), vibrational model of the azobenzene group in KCALP-azo.

Structural comparison of KCALP and KCALP-azo in dry POPC membranes

We gently dried POPC vesicles of reconstituted KALP, KCALP, and KCALP-azo peptides on the surface of a BaF_2 window, spontaneously forming oriented membranes (Figure 2A). Unpolarized FTIR absorption spectra for KCALP and KCALP-azo are presented in Figure 2B, which include the structure-sensitive backbone amide A (AA, νN−H), amide I (AI, νC = O), and amide II (AII, δN−H + νC−N) vibrations (Krimm and Bandekar, 1986), as well as νCH_2 and the ester νC = O vibrations from the lipids (Mantsch and McElhaney, 1991). The amide A, I and II vibration frequencies at 3296 cm^{-1}, 1659 cm^{-1}, and 1546 cm^{-1}, respectively, indicate that KCALP and KCALP-azo adopt, predominantly, an α-helical structure (Krimm and Bandekar, 1986). An amide I peak at a wavenumber as high as 1659 cm^{-1} has been only reported for TM helical peptides (Tamm and Tatulian, 1997), while for soluble α-helical peptides the amide I peaks at 1650-1644 cm^{-1} (Venyaminov and Kalnin, 1990). The observation in KCALP of a band at 2560 cm^{-1} from S-H vibrations, absent in KALP, confirmed that their Cys residues remain reduced before and after reconstitution in membranes (Figure S1A).

Figure 2C (top) expands the region between 1850 and 1510 cm^{-1} of KCALP and KCALP-azo, which includes the amide I and II vibrations. To resolve more details, we applied Fourier self-deconvolution (FSD) (Figure 2C, bottom), a mathematical tool for band-narrowing (Kauppinen et al., 1981). Note the high spectral similitude between KCALP-azo and KCALP for the amide I band after FSD, an indication that the photoswitch perturbs minimally the original structure of KCALP, as expected for an α-helical peptide with an azobenzene unit linked to *i* and *i*+11 cysteine residues (Flint et al., 2002). We also compared the 1850-1510 cm^{-1} region of KALP and KCALP (Figure S1B). The high spectral similarity indicates that the introduction of Cys residues in place of Ala is not particularly perturbative. The symmetric and rather narrow amide I and II bands from KCALP-azo, KCALP and KALP contrast with those from α-helix-rich membrane proteins (Figure S2), supporting a monomeric and homogeneous structure for the three peptides. As a final note, the band at 1597 cm^{-1} in KCALP-azo (see Figure 2C), absent in KCALP, can be assigned to νC = C vibrations of the azobenzene group (Pfister et al., 2008).

To obtain quantitative information about the secondary structure of KCALP and KCALP-azo, we decomposed their amide I and II envelops into sums of subcomponent bands by nonlinear least-squares. This decomposition is more robust when conducted on FSD spectra, in particular when using FSD-modified Gaussian, Lorentzian or Voigtian bands, instead of their conventional versions (Lórenz-Fonfría and Padrós, 2004a, 2004b). Figure 2D shows the band decomposition using FSD-modified Voigtian bands, and Tables S1 and S2 collect the estimated parameters for each fitted Voigtian band.

For an α-helix, amide vibrations couple into three vibrational modes, two of which are IR active: A and E_1 (Krimm and Bandekar, 1986). Because the A and E_1 modes strongly overlap for amide I vibrations, with a splitting of only ~2-7 cm^{-1} (Krimm and Bandekar, 1986; Marsh et al., 2000), they are observed as a single

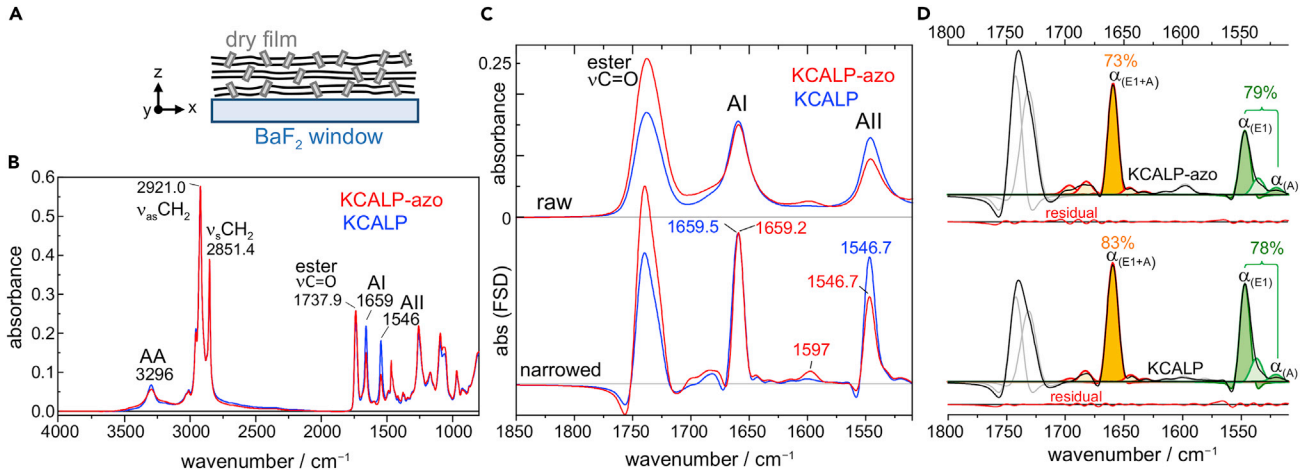

Figure 2. Structural comparison of KCALP and KCALP-azo in dried POPC membranes

(A) Sketch of oriented membranes.

(B) Unpolarized FTIR spectra of KCALP-azo (red) and KCALP (blue). Peptide backbone amide A (AA), amide I (AI), and amide II (AII) vibrations and lipid νCH_2 and ester $\nu C = O$ vibrations are labeled.

(C) Expanded 1850-1510 cm^{-1} region of the spectra in (B), before (top) and after (bottom) band-narrowing by FSD, scaled for the same amide I intensity. The band at 1597 cm^{-1}, present only in KCALP-azo, originates from the $\nu C = C$ of azobenzene.

(D) Band decomposition of FSD spectra using FSD-modified Voigtian bands (see Tables S1 and S2 for the band parameters). Bands in the 1700-1620 cm^{-1} region (red lines) and in the 1570-1515 cm^{-1} region (green lines) are assigned to amide I and amide II vibrations, respectively. Bands assigned to α-helices are color-filled (orange for amide I and olive for amide II bands), and their area percentages are indicated. Fitting residuals are shifted-down for clarity.

band at ~1659 cm^{-1} for both KCALP and KCALP-azo (Figure 2D). For the amide II vibration, the splitting of the E_1 and A modes is 20–30 cm^{-1} (Krimm and Bandekar, 1986; Marsh et al., 2000; Venyaminov and Kalnin, 1990), large enough to be well-resolved into two bands at ~1547 (E_1) and ~1520 (A) cm^{-1} (Figure 2D). The total band area assigned to helical structures in KCALP (color-filled bands in Figure 2D) corresponded to 83% and 78% of the total amide I and amide II area, respectively (Figure 2D, bottom). For KCALP-azo, on the other hand, these percentages were 73% and 79% (Figure 2D, top).

A more accurate estimation of the helical content of KCALP and KCALP-azo requires us to consider other groups with vibrations contributing to the amide I-II region. These include the NH_3^+ group from Lys, at ~1630 and ~1525 cm^{-1} in H_2O (Rahmelow et al., 1998); the secondary amide from the acetylated N-termini, at ~1630 cm^{-1} and ~1580 cm^{-1} in H_2O (Kubelka and Keiderling, 2001); and the primary amide from the amidated C-termini, at ~1670 cm^{-1} and ~1610 cm^{-1} in H_2O (Rahmelow et al., 1998). KCALP-azo contains two additional secondary amide groups located at the azobenzene linker (see Figure 1B), with expected bands at ~1700-1680 cm^{-1} and at ~1530-1500 cm^{-1} in aprotic organic solvents of low/medium polarity (Lorenz-Fonfria, 2020). Upon considering the expected wavenumber and absorption coefficient of these vibrations relative to those of the amide backbone group (Rahmelow et al., 1998), we concluded that both peptides are roughly 85% α-helical.

Despite the high resemblance between the vibrational spectra of KCALP and KCALP-azo, a good proxy for structural similarity, KCALP-azo displays an amide I/amide II intensity ratio notably higher than KCALP (Figure 2C). This observation suggests possible differences in the helix tilt of the two peptides with respect to the lipid membrane normal. To clarify this point, we conducted polarized-light FTIR experiments, presented in Figure S3, from where we estimated the average helix tilt, $\langle\beta\rangle$, to be $25.5^{28.7}_{20.5}{}^\circ$ for KCALP and $42.1^{43.7}_{40.2}{}^\circ$ for KCALP-azo. Thus, the coupling of azobenzene to KCALP does neither perturb its helical structure nor its TM topology, albeit it increases its average helix tilt by ~16.5°. Note that here, and throughout the text, we provide the most likely average tilt angle with an asymmetrical 96% confidence level. In some cases, however, we used for simplicity symmetrical confidence limits, e.g., $24.5 \pm 4^\circ$ instead of $25.5^{28.7}_{20.5}{}^\circ$.

Structure of KCALP-azo in hydrated POPC membranes

Films of KCALP-azo in POPC membranes were hydrated for all subsequent studies, either with ~450 (film A, Figure 3B) or with ~950 water molecules per peptide (film B, Figure S4). In either case, the lipid $\nu_s CH_2$

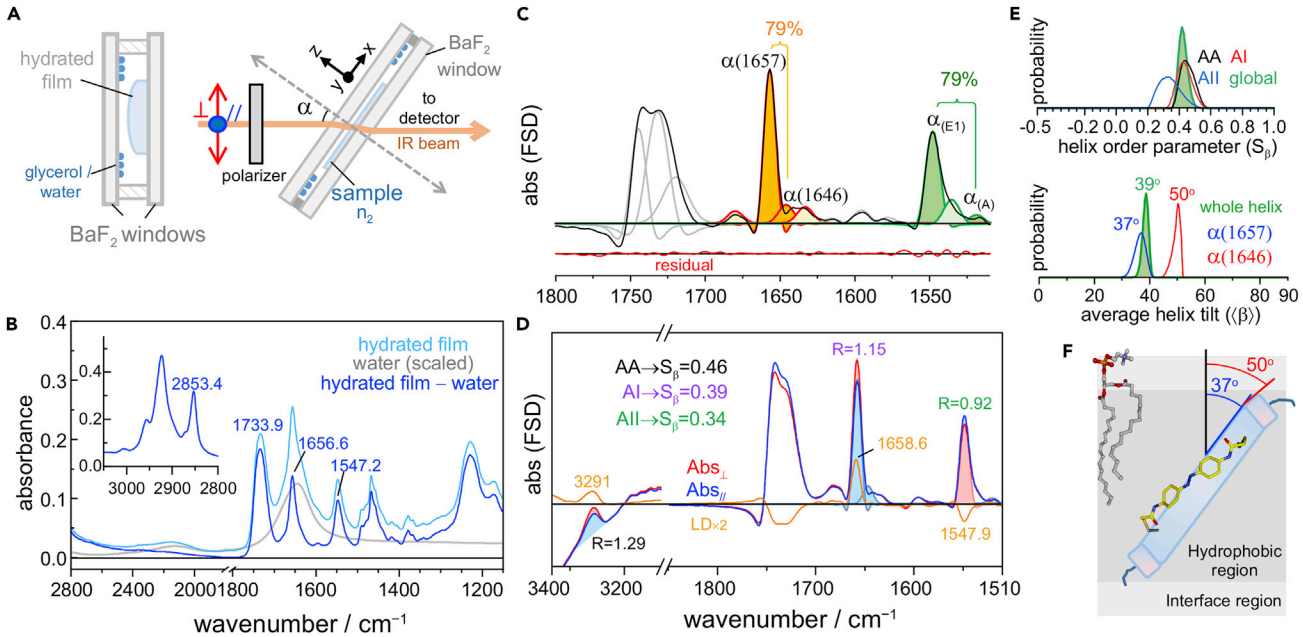

Figure 3. Structure and orientation of KCALP-azo in hydrated POPC membranes

(A) Schematic experimental setup.

(B) Unpolarized FTIR spectra of KCALP-azo before (light blue trace) and after (blue trace) subtraction of the water absorbance (gray trace).

(C) Band decomposition of the FSD spectrum of KCALP-azo (see Table S3).

(D) FSD polarized FTIR spectra of KCALP-azo (α = 50°). Dichroic ratios (R) from helices are given for each amide vibration, together with the second order parameter of the helix tilt (S_β). The LD spectrum is shown in orange, two times enlarged for clarity.

(E)(E, top) Probability distributions of S_β from each amide vibration (amide A, black; amide I, red; amide II, blue), and its global estimate (green, color-filled).

(E, bottom) Probability distributions of the average helix tilt for: the whole helix (green), and the helix segments corresponding to the bands at 1657 cm^{-1} (blue) and 1645 cm^{-1} (red).

(F) Schematic model of KCALP-azo in a hydrated POPC membrane, assuming a static helix tilt. The peptide helical structures are represented with cylinders. The hydrophobic core and interface regions of the lipid membrane are shown in gray and light gray, respectively, with a single POPC molecule depicted for illustration purposes.

vibration, at ~2853.4 cm^{-1} (insets in Figures 3B and S4), confirmed that the membranes were in the fluid phase (Mantsch and McElhaney, 1991). We digitally subtracted the background absorbance from liquid water, revealing the structure-sensitive amide I and amide II vibrations of the peptide backbone (Figures 3B and S4, blue trace). After FSD, the amide I and II bands of KCALP-azo peaked at 1656.8 ± 0.2 cm^{-1} and 1548.1 ± 0.2 cm^{-1}, respectively (Figure S5A).

To obtain a secondary structure estimate, we focused on film A because its lower water content made spectral corrections and the subsequent band-decomposition more reliable. The main amide I component band, with 66% of the area, is located at 1656.8 cm^{-1} (Figure 3C and Table S3), in the typical range for TM α-helices in proteins and in peptides (Goormaghtigh et al., 1994; Tamm and Tatulian, 1997). We assigned the band at 1646.0 cm^{-1}, with 13% of the area (Figure 3C and Table S3), to the amide I of hydrated α-helices (Lórenz-Fonfría et al., 2015; Walsh et al., 2003). The assignment of amide I bands at 1656.8 and 1646.0 cm^{-1} to helical structures is consistent with the band-decomposition of the amide II, giving a 79% of helical structures (Figure 3C and Table S3). We obtained comparable results for the hydrated film B (Table S4). Considering potential overlapping spectral contributions, discussed in the previous section, the estimated percentage of helical structures was ~85%. Therefore, the helicity of KCALP-azo does not significantly change upon hydration, although a portion of the TM helix, likely at the vicinity of the MI, becomes involved in H-bonds with interfacial water molecules.

Orientation of KCALP-azo in hydrated POPC membranes

We recorded FTIR absorption spectra using IR light with a polarization parallel ($Abs_{//}$) or perpendicular ($Abs_{\perp}$) to the axis of rotation of the sample window (Figure 3A). The resulting spectra were water-corrected and band-narrowed by FSD (Figure 3D). The linear dichroism spectrum (LD = $Abs_{\perp} - Abs_{//}$) shows a

positive amide A, a positive amide I, and a negative amide II band (Figure 3D, orange), similarly to KCALP-azo in dry POPC membranes (Figure S3B). This sign-pattern is characteristic for TM helical peptides (Ludlam et al., 1996) and proteins (Dave et al., 2008; DeLange and Bovee-Geurts, 1999; Earnest et al., 1990). In contrast, the pH-sensitive helical peptide LAH_4 displays the opposed sign-pattern when adopting an MI topology at low pH (Bechinger, 1996), as shown in Figure S3B (bottom).

To estimate the average helix tilt of KCALP-azo with respect to the membrane normal, $\langle\beta\rangle$, we first determined dichroic ratios, R, as the $Abs_{\perp}/Abs_{//}$ area ratio of amide vibrations from helical structures determined by band-fitting (Figure 3D). Then, we estimated the second order parameter of the helix tilt, defined as $S_{\beta} = \left(3\langle cos^2\beta\rangle - 1\right)/2$ (the brackets represent space and time-averaged values), using the following relation (Nabedryk and Breton, 1981; Rothschild and Clark, 1979):

$$S_{\beta} = \frac{n_2^2(R-1)}{3S_{ms}S_{\phi}sin^2\alpha + n_2^2(R-1)} \qquad \text{(Equation 1)}$$

In this equation, n_2 represents the refractive index of the hydrated film, S_{ms} its mosaic spread (i.e., the second order parameter of the lipid membrane normal with respect to the normal of the solid support), and S_{ϕ} the second order parameter of the angle between the transition dipole moment of an amide vibration and the helix axis. From the R values of the three amide vibrations (Figure 3D), and by considering the most likely values of the parameters involved in Equation 1, as well as their uncertainty (see STAR Methods), we obtained three probability distributions for S_{β} (Figure 3E-top, black, red, and blue traces). Combining them, we obtained a global estimate of $S_{\beta} = 0.41^{0.45}_{0.37}$ (Figure 3E, top, green trace). From the definition of S_{β} (see above) and applying the approximation $\langle cos^2\beta\rangle \approx cos^2\langle\beta\rangle$ (whose suitability is demonstrated below), we estimated the average helix tilt of KCALP-azo to be $38.6^{40.2^{\circ}}_{35.8^{\circ}}$ (Figure 3E, bottom, green trace). We also measured circular dichroism spectra of the oriented hydrated film of KCALP-azo, from 190 to 600 nm (Figure S6C). The obtained oriented circular dichroism (OCD) spectrum is fully consistent with KCALP-azo adopting a tilted helix in POPC membranes (Bürck et al., 2016).

KCALP-azo contains at least two distinguishable types of α-helices, resolved as two distinct amide I bands at ~1657 and ~1646 cm^{-1} (Figures 3C and Table S3). We were able to determine their individual dichroic ratios from the band-decomposition shown in Figure 3D (R = 1.17 and 1.08, respectively) and, thus, their average tilts ($36.7^{39.9^{\circ}}_{32.2^{\circ}}$ and $50.2^{51.6^{\circ}}_{46.0^{\circ}}$, respectively), as shown in Figure 3E (bottom, blue and red trace). Considering their wavenumbers (~1657 and ~1646 cm^{-1}), their average tilts (~37° and ~50°) and their relative areas (~70% and ~15%), we assigned the first of the two bands to the core segment of the TM-helix, and the second band to shorter helical segments at the peptide ends, near the interfacial region of the membrane, as schematically illustrated in Figure 3F.

As we have poited out before, we rely on the approximation $\langle cos^2\beta\rangle \approx cos^2\langle\beta\rangle$ to obtain average helix tilt values, β, from polarized IR experiments, i.e., we need to assume that $S_{\beta} \approx \left(3cos^2\langle\beta\rangle - 1\right)/2$. This approximation is only exact when the tilt angle takes a discrete value, which is not to be expected for helical peptides in membranes (Esteban-Martín et al., 2009; Ulmschneider et al., 2011). To evaluate the error made, we computed exact values for S_{β} and $<\beta>$ for a family of distributions of tilt angles (Figures S5A and S5B), and used the approximation $S_{\beta} \approx \left(3cos^2\langle\beta\rangle - 1\right)/2$ to determine back $\langle\beta\rangle$ from S_{β}. The discrepancy between exact and recovered values for $\langle\beta\rangle$ was <2.5° (in most cases <1°, Figure S5B), smaller than our statistical error, validating our approach to estimate $\langle\beta\rangle$ from experimental S_{β} values.

Photoisomerization of azobenzene in KCALP-azo

We determined that in hydrated POPC membranes ~85% of the backbone of KCALP-azo folds as an α-helix, the core of which (~70%) forms a TM hydrophobic segment with an average tilt of 36 ± 4°. In the following sections, we will focus on studying how photoisomerization of the covalently bound azobenzene group perturbs the structure and orientation of KCALP-azo in hydrated POPC membranes. But before that, we needed to establish to which degree we can photoisomerize the azobenzene moiety of KCALP-azo under our experimental conditions.

The UV-Vis absorption spectrum of KCALP-azo in hydrated POPC membranes (Figure 4A, red trace) shows a strong absorption band at 368 nm, characteristic for the electronic $\pi \rightarrow \pi^*$ transition of azobenzene in *trans* configuration (Beharry and Woolley, 2011). After UV illumination for 2 s (λ_{max} = 365 nm, 400 mW/cm^2), the absorption at 368 nm notably decreases, while the one at ~454 nm increases slightly (Figure 4A, blue trace), indicating a partial formation of the *cis* conformer of azobenzene (Beharry and Woolley, 2011).

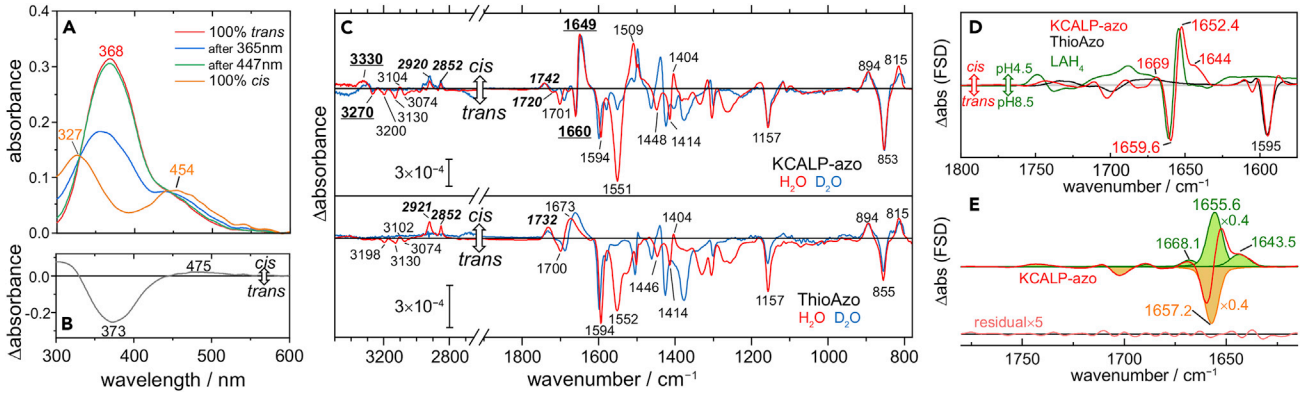

Figure 4. Light-induced changes after photoisomerization of KCALP-azo in hydrated POPC membranes

(A) UV-Vis absorption spectrum of dark-adapted KCALP-azo (100% *trans* conformation), after 365 nm (blue line), and after 447 nm (green line) illumination. The spectrum for 100% *cis* KCALP-azo (orange line) is an estimate.

(B) UV-Vis difference spectrum between *cis* and *trans* KCALP-azo.

(C)(C, top) Light-induced (365 nm-*minus*-447 nm) unpolarized FTIR difference spectra of KCALP-azo in membranes hydrated with H_2O (red trace) and D_2O (blue trace). The bands are labeled following their tentative assignment: peptide backbone (bold and underlined), lipid (bold and italics), and photoswitch (plain). (C, bottom) Light-induced FTIR difference spectra of ThioAzo in hydrated POPC membranes.

(D) Light-induced FTIR difference spectra of KCALP-azo (red) and ThioAzo (black), together with a scaled pH-induced FTIR difference spectrum of LAH_4 (green), all band-narrowed with FSD.

(E) Band-fitting of the FTIR difference spectrum of KCALP-azo in (D), with band parameters in Table S5. Note that the fitted bands at 1657.2 and 1655.6 cm^{-1} are scaled by 0.4 to keep their intensity within the displaying limits.

Blue illumination for 2 s (λ_{max} = 447 nm, 200 mW/cm^2) largely recovers the initial absorption spectrum (Figure 4A, green trace). A UV-Vis difference spectrum between the *trans* and *cis* conformers is shown in Figure 4B. Experiments made in parallel by FTIR difference spectroscopy confirmed that 2 s of illumination was sufficient to reach a photostationary state, PSS (Figure S8).

Because we could not fully drive KCALP-azo from *trans* to *cis* by illumination, we estimated the spectrum of *cis* KCALP-azo in hydrated POPC membranes by extrapolation (Figure 4A, orange trace). For that, we took as guidance the spectrum of 100% *cis* KCALP-azo measured in acetonitrile/water after its isolation by HPLC (Figure S9C). Then, considering that dark-adapted KCALP-azo is 100% *trans*, we estimated a 53% *cis*/47% *trans* PSS after 365 nm illumination, and a 4% *cis*/96% *trans* PSS after 447 nm illumination in POPC membranes. In other words, we could achieve a maximum of ~50% conversion between the *trans* and *cis* forms by alternating UV and blue light illumination. The above estimates are consistent with the PSS values determined for KCALP-azo in acetonitrile/water solution by HPLC: 2% *cis*/98% *trans* in the dark-adapted state, 48% *cis*/52% *trans* after 365 nm illumination, and 13% *cis*/87% *trans* after 447 nm illumination (Figure S9B).

Light-induced structural changes of KCALP-azo

UV-Vis spectroscopy confirmed the successful photoisomerization of the azobenzene group of KCALP-azo in hydrated POPC membranes, but it provided no clue about the accompanying structural changes in the peptidic part. Thus, we performed parallel experiments on the hydrated film B of KCALP-azo, measuring an FTIR difference spectrum after 2 s of UV illumination. The resulting spectrum was noisy, affected by a baseline drift, and included spectral signatures typical of sample heating (Figure S10B). To improve the spectral quality and to reduce heating artifacts, we alternated short light pulses of 365 nm (100 ms) and 447 nm (200 ms), repeating this cycle ~500 times, and averaging the result (see Figure S10A for a data acquisition scheme). The improvement in the spectral quality was remarkable (Figure S10B). As a drawback, the intensity of the light-induced FTIR difference spectrum of KCALP-azo decreased by a factor of ~2.5 (Figure S10B, red trace), *i.e.*, a reduction of the photoconversion between the *trans* and *cis* forms of KCALP-azo from a ~50% to a ~20%. This last difference FTIR spectrum is reproduced in Figure 4C (top, red trace). A similar light-induced FTIR difference spectrum was obtained for the hydrated film A (see Figure S5B).

Before interpreting the light-induced vibrational changes in KCALP-azo (Figure 4C, top), it was necessary to distinguish bands which originated from vibrations localized in the peptidic part from those coming from the azobenzene group. To achieve that, without resorting to complex and expensive isotope labeling, we

performed equivalent experiments on ThioAzo in POPC membranes (Figure 4C, bottom), used as a vibrational model of the azobenzene photoswitch in KCALP-azo (see Figure 1). Most of the bands in the light-induced FTIR difference spectrum of KCALP-azo are also present in ThioAzo, *i.e.*, they are assignable to vibrations localized in the azobenzene photoswitch. Among them, the bands at 1700 (−) and 1673 (+) cm^{-1} in ThioAzo and the band at 1701 (−) cm^{-1} in KCALP-azo (Figure 4C) can be assigned to amide I vibrations of the amide group at the photoswitch linker (see Figure 1), while the band at 1552 (−) cm^{-1} in ThioAzo and at 1551 (−) cm^{-1} in KCALP-azo (Figure 4C) likely correspond to amide II vibrations. The former bands downshifted by 10–13 cm^{-1} and the latter virtually vanished upon hydration with D_2O (Figure 4C, blue), as expected from their assignment (Lorenz-Fonfria, 2020). Given the known requirements for hydrogen/deuterium exchange, HDX (Englander et al., 2016), we can conclude that the two amide N−H groups at the photoswitch linker are largely free from H-bonding and, at least transiently, accessible to solvent water molecules.

Two intense bands at 1660 (−) and 1649 (+) cm^{-1} are observed only in the light-induced FTIR spectrum of KCALP-azo (Figure 4C, top), which can be assigned to changes in backbone amide I vibrations between the *trans* (unperturbed) and *cis* (perturbed) conformations of KCALP-azo. Likewise, two bands at ∼3330 (+)/∼3270 (−) cm^{-1} in KCALP-azo, absent in ThioAzo, can be assigned to changes in amide A vibrations of the peptide backbone. Very importantly, these backbone amide bands did not show up upon illumination of membranes containing equimolar quantities of KCALP and ThioAzo (Figure S11), meaning that illumination changed the structure of KCALP only when azobenzene was covalently bound to the peptide. Upon incubation of lipid-reconstituted KCALP-azo in D_2O, the backbone amide I bands downshifted by less than 2.5 cm^{-1} in the light-induced FTIR difference spectrum (Figure 4C top, compare red and blue traces), which contrasts with the expected 12 cm^{-1} downshift for a complete HDX (Lorenz-Fonfria, 2020). Therefore, most of the backbone amide N−H groups of KCALP-azo affected by illumination are HDX-resistant and, thus, involved in stable intramolecular H-bonding in both the unperturbed (*trans*) and perturbed (*cis*) states. Because D_2O removed amide II bands from the photoswitch but not from the peptide backbone, we could access changes from previously hidden backbone amide II vibrations (Figure 4C, blue traces). Only a small negative amide II band at ∼1550 cm^{-1} was observed, without any accompanying positive band (Figure 4C top, blue), indicating that the amide II vibration is largely insensitive to the structural changes caused by photoisomerization of KCALP-azo.

Although the 11 cm^{-1} downshift of the backbone amide I, from 1660 (−) to 1649 (+) cm^{-1}, might suggest a notable perturbation of the helical structure of KCALP-azo upon azobenzene photoisomerization, we should be aware that the apparent separation of bands with an opposed sign is always limited by their bandwidth (Grdadolnik, 2003). Indeed, after band narrowing by FSD, which reduces bandwidths, the same two bands were resolved only ∼7 cm^{-1} apart, at 1659.6 (−) and 1652.4 (+) cm^{-1} (Figure 4D). To resolve the bands contributing to the FTIR difference spectrum fully free from overlap effects, we relayed on band decomposition by nonlinear least-squares fitting. After this procedure, the two main amide I bands were resolved at 1657.2 (−) and 1655.6 (+) cm^{-1}, only 1.6 cm^{-1} apart (see Figure 4E and Table S5). The band-decomposition also revealed that both the position and width of the negative amide I band are quite close to those of the main amide I band in the absorbance spectrum of KCALP-azo (Table S5 *vs.* Table S4): 1657.2 *vs.* 1657.0 cm^{-1} and 14.2 *vs.* 16.6 cm^{-1}, respectively. This notable similitude favors the idea that the light-induced changes predominantly affect the hydrophobic segment of the TM helix of KCALP-azo.

To interpret the 1.6 cm^{-1} downshift of the amide I of KCALP-azo caused by light, we briefly moved our attention to the pH-sensitive helical peptide LAH_4. A dry film of POPC-reconstituted LAH_4 at pH 8.5, where the peptide is known to fully adopt a TM topology (Bechinger, 1996; Bechinger et al., 1999), displayed a main amide I band at 1658.1 cm^{-1} (Figure S12). The amide I maximum downshifted by 1.9 cm^{-1}, to 1656.2 cm^{-1}, at pH 4.5 (Figure S12), a condition where the peptide fully adopts an MI topology (Bechinger, 1996; Bechinger et al., 1999). The amide I frequency downshift can be explained by an increase of the medium polarity as the peptide moves to the MI at low pH (Oh et al., 2015). The amide II band of LAH_4 was largely insensitive to the change in membrane topology (Figure S12). In summary, the spectral differences in LAH_4 caused by a change in its membrane topology show a remarkable resemblance to those observed for KCALP-azo (compare red and green traces in Figure 4D), suggesting that KCALP-azo might experience a light-induced change in its membrane topology.

Although most of the area of the amide I band at 1657.2 cm^{-1} shifts to 1655.6 cm^{-1} upon azobenzene photoisomerization, part of it also shifts to 1643.5 and 1668.1 cm^{-1} (Figures 4D and 4E and Table S5). The

positive amide I band at 1643.5 cm^{-1} is akin to the band at 1645.6 cm^{-1} in the FTIR absorption spectrum of KCALP-azo (Figure 3C and Table S4), indication that part of the TM helical segment might establish H-bonds with water after adopting an MI topology. On the other hand, the positive amide I band at 1668.1 cm^{-1} might originate from weakly H-bonded backbone amide carbonyl groups (Lorenz-Fonfria, 2020), formed as a result of structural distortions in the TM helical segment of KCALP-azo.

Light-induced changes in the helix tilt of KCALP-azo

In order to detect changes in the tilt of the helix of KCALP-azo, we first performed light-induced polarized FTIR difference spectroscopy in combination with attenuated total reflection (ATR). We conducted these experiments on oriented films hydrated with D_2O, providing access to amide A, I and II bands from the peptide. Changes in the helix tilt can be easily gauged by transforming polarized ATR-FTIR difference spectra ($\Delta Abs_{\perp}$ and $\Delta Abs_{//}$) into difference spectra in the plane ($\Delta Abs_{x\text{-}y}$) and perpendicular (ΔAbs_z) to the surface of the ATR crystal (Lorenz-Fonfria et al., 2009), see Figure 5A (inset). In addition, an isotropic difference spectrum, ΔAbs_{iso}, free from orientation effects, is obtained as: $\Delta Abs_{iso} = (\Delta Abs_z + 2\times\Delta Abs_{x\text{-}y})/3$ (Lorenz-Fonfria et al., 2009). To explain how $\Delta Abs_{x\text{-}y}$ and ΔAbs_z help to detect changes in the tilt of helices, Figure 5A includes cartoons of a simple idealized helix changing its tilt from 0° to 90° with respect to the *z* axis. When the transition dipole moment aligns close to the direction of the helix axis, like for the amide A, ϕ = 27-33° (Marsh et al., 2000; Marsh and Páli, 2001; Tsuboi, 1962), a larger helix tilt causes the absorption to decrease in the *z* direction and to increase in the *x-y* plane, leading to a negative band in the ΔAbs_z spectrum and a positive band in the $\Delta Abs_{x\text{-}y}$ spectrum (Lorenz-Fonfria et al., 2009). This was indeed the observed pattern for the amide A band of KCALP-azo (Figure 5A, green shaded area), compelling evidence for an increased helix tilt upon *trans*-to-*cis* azobenzene photoisomerization. Being the transition dipole moment of the amide II close to perpendicular to the helix axis, ϕ = 70-76° (Marsh et al., 2000; Marsh and Páli, 2001; Tsuboi, 1962), a larger helix tilt should raise the absorption in the *z* direction while decreasing it in the *x-y* plane. Indeed, we observe a positive amide II band in the ΔAbs_z spectrum and a negative one in the $\Delta Abs_{x\text{-}y}$ spectrum (Figure 5A, orange shaded area), further confirming a light-induced increase of the helical tilt of KCALP-azo.

Only the amide I frequency of the helix changed sufficiently with the tilt as to resolve both positive (*cis*) and negative (*trans*) bands in both ΔAbs_z and $\Delta Abs_{x\text{-}y}$. Because the negative band was more intense in ΔAbs_z than in $\Delta Abs_{x\text{-}y}$, but it was the other way around for the positive band, we can conclude that the helix tilt of KCALP-azo is smaller than the magic angle (54.7°) after blue illumination (*trans* azobenzene) but larger than the magic angle after UV illumination (*cis* azobenzene). To obtain quantitative values for the helix tilt, we conducted additional light-induced polarized FTIR difference experiments, but this time by transmission and with samples hydrated with H_2O (Figure 5B). We determined the dichroic ratio of the negative and positive amide I bands by integrating their area after FSD (Figure 5B, inset). For the negative band, *R* was 1.21, and we arrived at $S_\beta = 0.55^{0.68}_{0.46}$, and finally to $\langle\beta\rangle = 33.1^{37.0°}_{27.3}$ (Figure 5C, red). This latter estimate is in statistical agreement with the average helix tilt determined for the hydrophobic TM helical segment of KCALP-azo in the dark, $36.7^{39.9°}_{32.2}$ (Figure 3E, bottom, blue trace), indicating that this is the segment of KCALP-azo whose tilt is perturbed by light.

From the dichroic ratio of the positive band, 0.89 (Figure 5B, inset), we arrived at $S_\beta = -0.44^{-0.34}_{-0.49}$ and at $\langle\beta\rangle = 77.3^{87.3°}_{71.0}$ for *cis* KCALP-azo (Figure 5C, blue). Figure S7D displays several distributions of β compatible with $S_\beta = -0.44$, spanning from a perfectly homogeneous helix tilt of $\beta \approx 77°$ to a broad Gaussian distribution of β angles centered at ~90°. Note that a helix tilt equal to or higher than 77° for a 24 residue-long peptide appears incompatible with a TM topology, even if considering possible snorkelling effects of the Lys charged residues in the helix termini. Instead, this tilt agrees well with those previously described for MI helical peptides (Mayo et al., 2018; Strandberg et al., 2016; Tucker et al., 2004; Whiles et al., 2001). Incidentally, the positive band at 1643.5 cm^{-1} (Figure 4E), assigned to hydrated helical segments (see above), displayed a dichroic ratio of 0.98 (Figure 5B, inset), from where we estimated its average helix tilt to be $56.8^{60.0°}_{54.8}$.

Figure 5D shows two structural models for the MI state of *cis* KCALP-azo compatible with our experimental results. The first model is a V-shaped helical conformation with a static orientation (Figure 5D, top). The second model the helix exhibits a dynamic orientation, fluctuating between a flat alignment at the MI and a V-shaped conformation (Figure 5D, bottom). Both models can explain the average tilt of the hydrophobic helix segment of *cis* KCALP-azo (~77°). Although we lack direct information about the peptide azimuthal

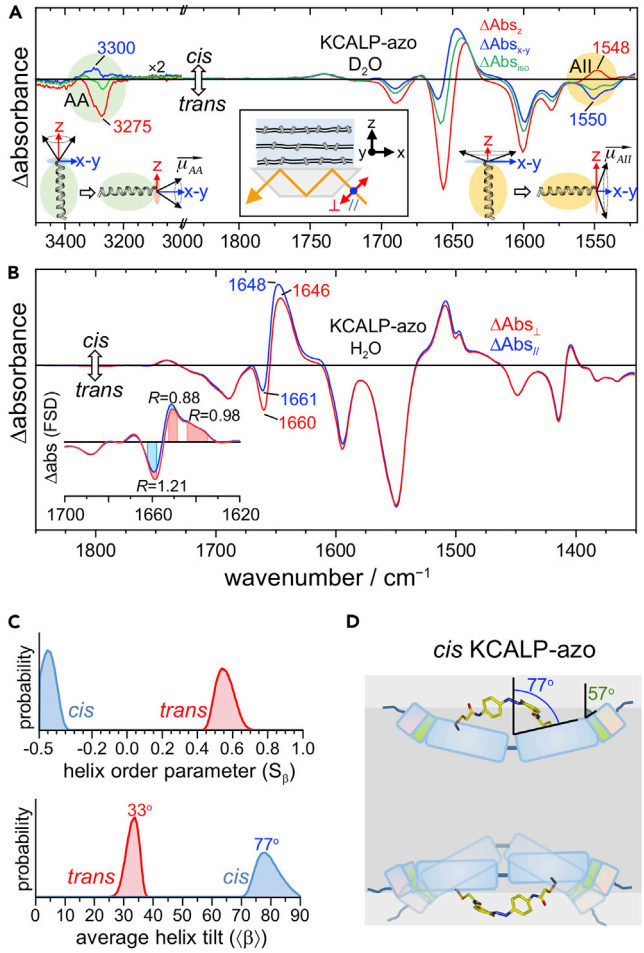

Figure 5. Light-induced orientation changes of the α-helix of KCALP-azo in hydrated POPC membranes

(A) Light-induced FTIR difference spectra in D_2O in the plane ($\Delta Abs_{x\text{-}y}$, red) and perpendicular to the sample surface (ΔAbs_z, blue), obtained by ATR with polarized light (see inset). ΔAbs_{iso} (green) is the isotropic difference spectrum. Changes in $\Delta Abs_{x\text{-}y}$ and ΔAbs_z for the amide A (green-shared area) and amide II (orange-shaded area) bands indicate an increase of the helix tilt of KCALP-azo upon *trans*-to-*cis* photoisomerization. For clarity, the tilt increase is illustrated with cartoons showing a 0°–90° change.

(B) Light-induced polarized FTIR difference spectra in H_2O, measured by transmission ($\alpha = 50°$). The inset shows the amide I region after FSD. The dichroic ratio, *R*, for two positive bands (*cis* state) and one negative band (*trans* state) is indicated.

(C) Probability distributions for the second order parameter (top) and for the average tilt angle (bottom) of the main helix segment of KCALP-azo in *trans* (red) and *cis* (blue) conformations.

(D) Schematic structural model of *cis* KCALP-azo. Helical segments are shown as cylinders, color-coded according to their amide I frequency and average tilt: 1655.6 cm^{-1}/77° (light blue), 1643.5 cm^{-1}/57° (light green), and 1646 cm^{-1}/50° (light red). The latter component is preserved from *trans* KCALP-azo and reproduced from Figure 3F.

rotation, we tentatively placed it facing the MI region, after considering that the polarity of azobenzene markedly increases in its *cis* isomeric state (Szymański et al., 2013).

Fraction of KCALP-azo moving to the MI after azobenzene photoisomerization

We reconstructed the FTIR absorption spectrum of pure *cis* KCALP-azo by considering that, under our illumination conditions, the change in the isomeric state of azobenzene occurs only for ~20% of the KCALP-azo molecules. This was done by simply adding to the FTIR absorption spectrum of dark-adapted KCALP-azo (100% *trans*), the light-induced FTIR difference spectrum multiplied by 5. The resulting 100% *cis* spectrum, presented in Figure 6A after FSD, displays the expected reduction in the intensity of the 1596 cm^{-1} band from the νC = C of azobenzene (Denschlag et al., 2010). However, the amide I band downshifts by only 0.16 cm^{-1}. In contrast, for LAH_4, the amide I downshifts by ~1.9 cm^{-1} from the TM to the MI state (Figure S12),

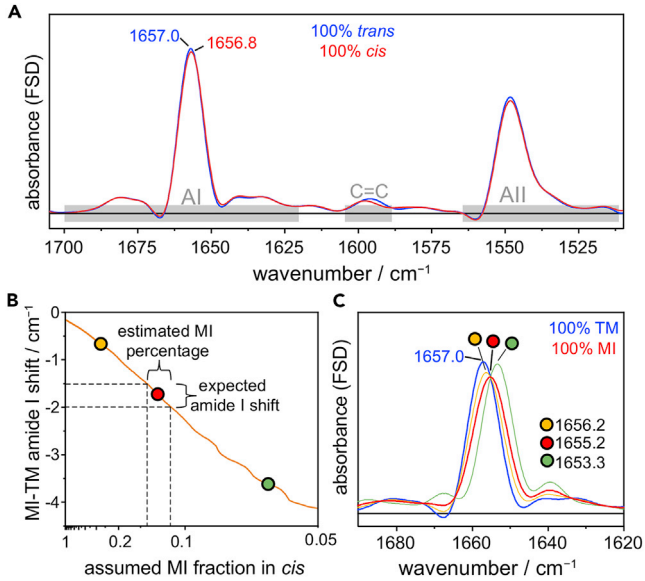

Figure 6. Mixture of TM and MI states in *cis* KCALP-azo

(A) FSD absorption spectrum of 100% *trans* KCALP-azo, adopting a 100% TM state (blue, reproduced from Figure S5A). Estimated absorption spectrum of 100% *cis* KCALP-azo (red). The small downshift of the amide I, 0.2 cm^{-1}, indicates that *cis* KCALP-azo exists in a TM and MI mixture.

(B) Downshift of the amide I band maximum between the 100% MI spectrum (estimated with Equation 3) and the 100% TM spectrum (taken from 100% *trans* KCALP-azo) as a function of the value assumed for f_{cis}^{MI} (fraction of *cis* KCALP-azo in the MI state). From the expected MI-TM amide I band downshift, 1.5–2.0 cm^{-1} (dashed horizontal lines), we obtained an estimate of 0.14–0.11 for f_{cis}^{MI} (dashed vertical lines). Three values for f_{cis}^{MI} are labeled: optimal (red), overestimated (orange) and underestimated (green).

(C) Amide I spectrum of KCALP-azo in a 100% TM state (blue, same as in (A)) and in a 100% MI state (red), the latter reconstructed assuming *cis* KCALP-azo to be 88% TM and 12% MI. Reconstructions of the 100% MI spectrum assuming f_{cis}^{MI} = 0.24 (orange) or f_{cis}^{MI} = 0.06 (green), display an amide I downshift smaller (0.8 cm^{-1}) or larger (3.7 cm^{-1}) than expected.

and our band decomposition analysis for KCALP-azo suggests the amide I downshift between the MI and TM states to be ~1.6 cm^{-1} (Figure 4E). Furthermore, the OCD spectrum for *cis* KCALP-azo is barely distinguishable from that of *trans* KCALP-azo (Figure S6C). These observations indicate that the FTIR (and OCD) spectra of *cis* KCALP-azo, Abs_{cis}, arise from a mixture of TM and MI states:

$$Abs_{cis} = \left(1 - f_{cis}^{MI}\right) Abs_{cis}^{TM} + f_{cis}^{MI} Abs_{cis}^{MI} \qquad \text{(Equation 2)}$$

being the TM state the dominant one. To estimate the amide I spectrum of *cis* KCALP-azo in the MI state, Abs_{cis}^{MI}, we assumed that the amide I spectrum depends on the membrane topology adopted by the peptide but it is not significantly affected by the isomeric state adopted by the azobenzene moiety, *i.e.*, $Abs_{cis}^{TM} \approx Abs_{trans}^{TM}$. After considering that *trans* KCALP-azo is 100% TM, *i.e.*, $Abs_{trans} = Abs_{trans}^{TM}$, and rearranging Equation 2, we arrived to:

$$Abs_{cis}^{MI} \approx \frac{Abs_{cis} - Abs_{trans}\left(1 - f_{cis}^{MI}\right)}{f_{cis}^{MI}} \qquad \text{(Equation 3)}$$

Using this equation, we estimated Abs_{cis}^{MI} for different values of f_{cis}^{MI}, the fraction of *cis* KCALP-azo in an MI state. Figure 6B plots how much the amide I downshifts between the MI and TM states of KCALP-azo as a function of the value assumed for f_{cis}^{MI}. Because we expect this downshift to be around 1.5–2.0 cm^{-1}, we deduced that f_{cis}^{MI} takes a value between 0.11 and 0.14 (see Figure 6B, dashed lines), *i.e.*, ~11-14% of *cis* KCALP-azo adopts an MI state. As an illustration, Figure 6C shows the reconstructed amide I spectrum for the MI state, estimated using f_{cis}^{MI} = 0.12 (red trace). The same plot shows, for reference, a reconstruction using a twice-larger (orange trace) or a twice-smaller (green trace) value.

We obtained an additional estimation for f_{cis}^{MI}. The area of the negative band at 1657.2 cm^{-1} in the light-induced FTIR difference spectrum (Figure 4E and Table S5) is 60 times smaller than the area of the positive

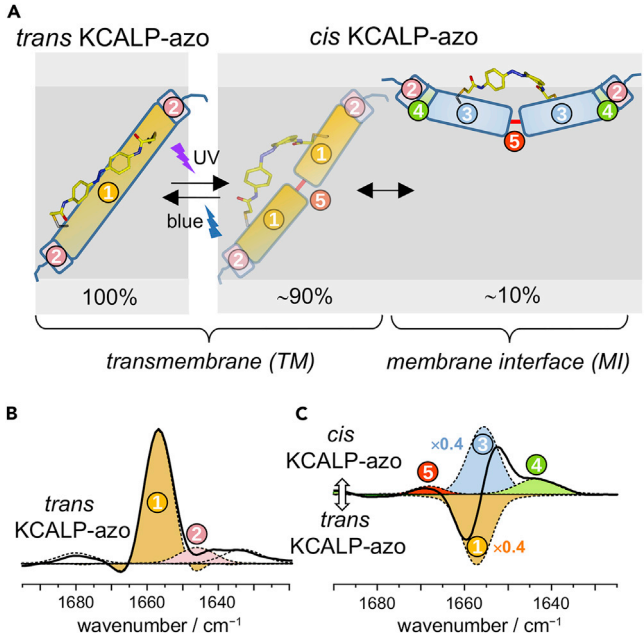

Figure 7. Structural models of the photoswitchable peptide KCALP-azo in *trans*-azobenzene-TM and *cis*-azobenzene-TM/MI states

(A) Structure and membrane topology of KCALP-azo when the azobenzene group is in either *trans* (left) or *cis* (right) isomeric state. The helical peptide structures are illustrated as cylinders, tilted according to the experimental results (azimuthal rotation angles are tentative).

(B) Band-narrowed FTIR absorption spectrum of *trans* KCALP-azo, with its component bands resolved by band-fitting.

(C) Band-narrowed light-induced FTIR difference spectrum of KCALP-azo (*cis* minus *trans*), with its component bands resolved by band-fitting. Related structural/spectral elements in (A-C) are labeled using common colors and number codes.

band at 1657.0 cm^{-1} in the FTIR absorption spectrum of *trans* KCALP-azo (Figure 3C and Table S4). From this result, and taking into account that only 20% of the azobenzene groups were photoisomerized, we inferred that just 8% of KCALP-azo changed to an MI topology when photoisomerized. Thus, two different lines of reasoning indicate that *cis* KCALP-azo exists as a mixture of ~90% TM and ~10% MI states.

DISCUSSION

The coupling of azobenzene to Cys side chains has been one of the approaches used in the past to introduce structural perturbations on soluble helical polypeptides with light (Albert and Vázquez, 2019; Beharry and Woolley, 2011; Hamm et al., 2008; Szymański et al., 2013). Here, we have extended this approach to KCALP-azo, a 24 residues-long TM-helical peptide. First, we characterized the structure and orientation of KCALP-azo in its dark-adapted state (~100% *trans* isomer). We have confirmed that KCALP-azo is indeed a TM and highly helical (~85%) peptide (Figure 3). In addition, we found that *trans* KCALP-azo displays two types of helical segments with distinct properties. The dominant helix type (~70%) displays an amide I frequency at 1657 cm^{-1}, characteristic for α-helices in TM proteins and peptides (Goormaghtigh et al., 1994; Tamm and Tatulian, 1997) and shows an average tilt of 36 ± 4° (Figure 3, and ① in Figure 7B). We assign it to the core of the TM helix of KCALP-azo (① in Figure 7A). The minor helix type (~15%) displays an amide I frequency at 1646 cm^{-1}, characteristic for helices forming bifurcated H-bonds with water molecules (Lórenz-Fonfría et al., 2015; Walsh et al., 2003) and shows an average tilt of 49 ± 3° (Figure 3, and ② in Figure 7B). Thus, it likely corresponds to short segments at the two ends of the TM helix (② in Figure 7A).

We next studied changes in the structure and orientation of KCALP-azo after being exposed to alternating UV and blue light pulses, which converts 20% of the azobenzene groups from a *trans* to a *cis* conformation. In the FTIR difference spectrum, the band at 1657.2 cm^{-1} represents 99% of the negative amide I area (① in Figure 7C, see also Figure 4E and Table S5), and shows a frequency and width very similar to the amide I band at 1657.0 cm^{-1} in the absorbance spectrum of KCALP-azo (① in Figure 7B, see also Table S4). This

high similitude indicates that photoisomerization of the azobenzene moiety affects almost exclusively the hydrophobic core-segment of the TM helix of KCALP-azo. On the other hand, we observed three positive amide I bands in the light-induced FTIR difference spectrum of KCALP-azo (Figure 4E). The main positive band (1655.6 cm^{-1}) accounts for 86% of the amide I area (③ in Figure 7C, see also Figure 4E and Table S5), and it originates from the amide I vibration of a helix tilted by ~79 ± 8° with respect the membrane normal (Figure 5). Thus, azobenzene photoisomerization causes the central TM hydrophobic segment of KCALP-azo to change, both in amide I frequency (from ~1657.2 cm^{-1} to ~1655.6 cm^{-1}) and in average tilt (from 36 ± 4° to 79 ± 8°), as illustrated in Figure 7 (see ① to ③).

Although the helix tilt angle of a peptide does not directly define its topology in the membrane, it certainly constrains it. Considering the hydrophobic thickness of POPC in fluid phase, ~29 Å (Kučerka et al., 2011), a TM topology with an average helix tilt of 79 ± 8° can be discarded just from energetic considerations, as it would involve placing at least two of the four positively charged Lys residues of KCALP-azo (Figure 1B) within the hydrophobic region of the membrane. The helix tilt of ~79 ± 8° for the MI state of *cis* KCALP-azo agrees well with that of mastoparan X, a helical peptide adopting MI topology, with a tilt angle determined to be 80 ± 5° by NMR (Whiles et al., 2001) and 76 ± 7° by FTIR spectroscopy (Tucker et al., 2004). In addition, the shift in the amide I frequency between bands ① and ③ (Figure 7C) is very similar to the shift that we observed between the TM and MI states of the pH-sensitive helical peptide LAH_4 (Figure S12).

The migration of KCALP-azo to the interface of the membrane goes accompanied by an enlargement of its hydrated helical segment (see ④, Figure 7A), as indicated by the positive band at 1643.5 cm^{-1} (④ in Figure 7C, see also Table S5). Finally, we also have a small positive band at 1668 cm^{-1} (⑤ in Figure 7C, see also Table S5). Although the assignment of this band is tentative, given its wavenumber it might originate from weakly H-bonded backbone peptide groups formed because of a distortion of the TM helix by *trans*-to-*cis* photoisomerization. We postulate that such distortion might localize near the center of the helix core (⑤ in Figure 7A), allowing for a bend in the TM helix in response to *trans*-to-*cis* isomerization of azobenzene.

The changes reported here for KCALP-azo are drastically different from those reported before for photoswitchable soluble helical peptides. As an example, azobenzene *trans*-to-*cis* photoisomerization was shown to almost completely unfold a 16 residue-long soluble helical peptide, reducing its helix content from 93% (*trans*) to 34% (*cis*) (Bredenbeck et al., 2005). Why does a photoswitchable hydrophobic helical peptide reconstituted in membranes respond so differently to light? We must take into account that the energetic cost for breaking a backbone amide H-bond in the hydrophobic core of lipidic membranes, +4-5 kcal/mol (Bolen and Rose, 2008; White and Wimley, 1999), is much higher than in aqueous solution, +0.5–1 kcal/mol (Bolen and Rose, 2008). As a result, it is expected that photoisomerization of azobenzene will not induce the unfolding of a TM helix to any degree close to that reported before for soluble peptides. In agreement, our observations show that KCALP-azo largely preserves its helical structure upon *trans*-to-*cis* photoisomerization.

To understand why azobenzene photoisomerization induced a change in the membrane topology of KCALP-azo, we need to be aware that the energetically closest state to a TM helix is not an unfolded TM state but rather a helix located at the interface of the membrane (White and Wimley, 1999). From the sequence of KCALP, and using the hydrophobicity scales from Wimley and White (Wimley et al., 1996; Wimley and White, 1996), implemented in the MPEx tool (Snider et al., 2009), we estimated the free energy difference between its TM and MI states, hereafter $\Delta G^{\circ}_{TM\text{-}MI}$, to be −4.5 kcal/mol. For this estimate, we considered only residues from Leu4 to Leu21, because we expect the three residues at either peptide end (GKK at the N-terminus and KKA at the C-terminus) to face the interface of the membrane, regardless of the membrane topology adopted by KCALP. For KCALP-azo, it is not possible to estimate $\Delta G^{\circ}_{TM\text{-}MI}$ from MPEx, but it is plausible that both KCALP and *trans* KCALP-azo share a similar $\Delta G^{\circ}_{TM\text{-}MI}$ when considering that both peptides show a similar elution time (*i.e.*, hydrophobicity) on an HPLC C8 column (see Figures S13A and S15A). The $\Delta G^{\circ}_{TM\text{-}MI}$ value provided by MPEx is sufficiently favorable to ensure that virtually 100% of KCALP (and *trans* KCALP-azo) adopts a TM topology, yet sufficiently low for changes in noncovalent interactions to significantly modulate the TM propensity of this peptide. The experimentally estimated TM/MI equilibrium constant for *cis* KCALP-azo, ~90/10 = 9, indicates a $\Delta G^{\circ}_{TM\text{-}MI}$ of −1.3 kcal/mol. This value suggests that azobenzene *trans*-to-*cis* photoisomerization can increase $\Delta G^{\circ}_{TM\text{-}MI}$ of KCALP-azo by ~3.2 kcal/mol (from −4.5 to −1.3 kcal/mol). Because breaking an intramolecular H-bond

costs 3-4 kcal/mol less at the MI than at the hydrophobic region of the membrane (White and Wimley, 1999), we propose that azobenzene photoisomerization breaks (or weakens) one or more intramolecular H-bonds of KCALP-azo, favoring the peptide migration to the MI. In addition, we should not forget that the higher polarity of *cis* azobenzene compared with the *trans* isomer (Beharry and Woolley, 2011) might also contribute to stabilize the MI state. Indeed, *cis* KCALP-azo is more polar than *trans* KCALP-azo, as indicated by the earlier elution time of the former in an HPLC C8 column (Figure S9B).

Although our experimental data clearly points to a change in the membrane topology of KCALP-azo upon azobenzene photoisomerization, this change in topology is far from complete. We roughly estimated that only ~10% of those peptides with the azobenzene group in *cis* conformation experienced a change in membrane topology (Figure 6). Consequently, the measured static light-induced FTIR difference spectrum of KCALP-azo (Figure 4C) actually represents a mixture of two different spectra: ($Abs^{TM}_{cis} - Abs^{TM}_{trans}$) and ($Abs^{MI}_{cis} - Abs^{TM}_{cis}$). Future time-resolved experiments should be able to disentangle these two spectral contributions because structural changes that immediately follow the photoisomerization of the azobenzene ($Abs^{TM}_{cis} - Abs^{TM}_{trans}$) are expected to occur much earlier than the changes associated with variations of the membrane topology ($Abs^{TM}_{cis} - Abs^{TM}_{cis}$).

The possibility of repetitively perturb with light the MI/TM equilibrium of a peptide, even by a small degree as reported here, will make it much easier to follow the membrane insertion of a peptide by time-resolved methods. One example is time-resolved FTIR spectroscopy, rich in structural and dynamic information (Kottke et al., 2017; Lorenz-Fonfria, 2020). Note that time-resolved studies achieve the highest possible temporal resolution when they can use laser pulses as a trigger. In addition, they achieve the highest possible quality when studying reversible systems, which grants extensive data averaging with minimal sample consumption. Consequently, a peptide with a membrane topology that can be reversibly controlled by light, such as KCALP-azo, seems ideally suited for time-resolved experiments addressing the sequence of events that allow peptides (and protein fragments) to spontaneously insert into or move out of membranes.

The low TM-to-MI photoconversion reported here for KCALP-azo might have some advantages for future time-resolved experiments, limiting changes in the properties of the lipidic membrane that might complicate their analysis and interpretation. Indeed, in our static light-induced FTIR difference spectra, we could observe only tiny bands assignable to changes in lipid vibrations (Figure 4C), indicating that the main physical properties of the POPC bilayers, like phase and fluidity, were not significantly altered.

The optical control of the membrane topology of peptides might also be the starting point for interesting applications. For instance, the pH-sensitive peptide pHLIP can deliver polar molecules toward the interior of cells in response to a MI-to-TM reorientation change induced at low pH, a property used to target drugs to tumor cells (Wyatt et al., 2018). Likewise, light control of the membrane topology of peptides could allow for the delivery of small molecules by the same mechanism as for pHLIP, *i.e.*, transport of small cargo molecules without peptide penetration into the cell, although with the added benefits in temporal and spatial resolution that light provides.

Limitations of the study

The main limitation of the present study is the low photo-conversion from a TM to a MI topology achieved for KCALP-azo. Under our experimental illumination conditions, only 20% of KCALP-azo photoisomerized from the *trans* to the *cis* state and, from this 20%, only ~10% changed its membrane topology. Thus, in practice, only ~2% of the total peptide switched with light from a TM to an MI state. Although this small percentage did not represent a serious limitation for our sensitive FTIR difference spectroscopic experiments, it prevents the application of other techniques sensitive to orientation, like solid-state NMR or OCD, to resolve them. The low photo-perturbation of the membrane topology reported here is also a serious limitation for future molecular strategies aiming to exploit it for practical purposes. Thus, future efforts should focus on enhancing the conversion of the TM to the MI state with light. One possibility is to explore if, by including changes in the chemical nature of the photoswitch or in its coupling to the peptide, we could increase the TM-MI photo-conversion. Another possibility that we are currently exploring is increasing the polarity of the scaffold peptide to facilitate its migration to the MI. As an example, exchanging two Leu residues by Ala in the primary structure of KCALP is expected to increase $\Delta G^{\circ}_{TM\text{-}MI}$ by ~2 kcal/mol (Snider et al., 2009). Extrapolating this prediction to KCALP-azo, we predict a $\Delta G^{\circ}_{TM\text{-}MI}$

of −2.5 kcal/mol for the *trans* conformation (TM/MI of ~99%/1%) and +0.7 kcal/mol for the *cis* conformation (TM/MI ~25%/75%), *i.e.*, a potential 74% change of the membrane topology with light.

Another limitation of the present study is that it was unable to provide experimental information about the azimuthal rotation angle for the helix of KCALP-azo in the TM and MI states. This angle might not be very relevant for the TM state, but for the MI state the azimuthal rotation angle defines which residues face the interface region of the membrane, as well as the location of the azobenzene group. At present, we consider that it is most reasonable to assume that the azobenzene group faces the MI in the MI state, as illustrated in Figure 7. In the future, direct information about the azimuthal rotation angle of KCALP-azo in its MI state could be obtained, for instance, by polarized FTIR experiments in combination with a suitable site-specific labeling strategy, following the work by Arkin and coworkers (Arkin, 2006).

STAR★METHODS

Detailed methods are provided in the online version of this paper and include the following:

- KEY RESOURCES TABLE
- RESOURCE AVAILABILITY
  - Lead contact
  - Materials availability
  - Data and code availability
- METHODS DETAILS
  - Peptide synthesis and purification
  - Synthesis of KCALP-azo, BCA and ThioAzo
  - Peptide reconstitution in POPC membranes
  - Preparation and characterization of oriented films
  - FTIR measurements
  - UV-Vis measurements
  - OCD measurements
- QUANTIFICATION AND STATISTICAL ANALYSIS
  - Spectral analysis
  - Determination of helical tilts

SUPPLEMENTAL INFORMATION

Supplemental information can be found online at https://doi.org/10.1016/j.isci.2021.102771.

ACKNOWLEDGMENTS

We thank the financial support provided by the Ministerio de Ciencia e Innovación (MICINN) - Agencia Estatal de Investigación (AEI) through projects BFU2016-768050-P, BFU2017-91559-EXP, PID2019-106103GB-I00 and CTQ2017-87372-P, and by the Generalitat Valenciana through the project PROMETEU/2019/066. V.A.L.-F acknowledges a Ramon y Cajal fellowship (RYC-2013-13114), M.G.-S. a predoctoral fellowship (BES-2017-080385) from the MICINN, and E.S.-A. a predoctoral fellowship from Universidad de La Rioja. V.A.L.-F. is in debt with Joachim Heberle for access to a Vertex 80v FTIR spectrometer in the early stage of this work, and thanks Mattia Saita and Franziska Sellnau for assistance during those measurements.

AUTHOR CONTRIBUTIONS

D.S. and V.A.L.-F. designed the research; M.G.-S., E.S.-A., L.S., and V.A.L.-F. performed experiments and analyzed data; M.G.-S., E.S.-A., D.S., J.S., and V.A.L.-F. discussed the results and wrote the paper.

DECLARATION OF INTERESTS

There are no conflicts to declare.

Received: April 9, 2021
Revised: June 2, 2021
Accepted: June 19, 2021
Published: July 23, 2021

REFERENCES

Albert, L., and Vázquez, O. (2019). Photoswitchable peptides for spatiotemporal control of biological functions. Chem. Commun. *55*, 10192–10213. https://doi.org/10.1039/C9CC03346G.

Andreev, O.A., Karabadzhak, A.G., Weerakkody, D., Andreev, G.O., Engelman, D.M., and Reshetnyak, Y.K. (2010). pH (low) insertion peptide (pHLIP) inserts across a lipid bilayer as a helix and exits by a different path. Proc. Natl. Acad. Sci. U S A *107*, 4081–4086. https://doi.org/10.1073/pnas.0914330107.

Arkin, I.T. (2006). Isotope-edited IR spectroscopy for the study of membrane proteins. Curr. Opin. Chem. Biol. *10*, 394–401.

Babii, O., Afonin, S., Berditsch, M., Reiβer, S., Mykhailiuk, P.K., Kubyshkin, V.S., Steinbrecher, T., Ulrich, A.S., and Komarov, I.V. (2014). Controlling biological activity with light: diarylethene-containing cyclic peptidomimetics. Angew. Chem. *126*, 3460–3463. https://doi.org/10.1002/ange.201310019.

Babii, O., Afonin, S., Ishchenko, A.Y., Schober, T., Negelia, A.O., Tolstanova, G.M., Garmanchuk, L.V., Ostapchenko, L.I., Komarov, I.V., and Ulrich, A.S. (2018). Structure–activity relationships of photoswitchable diarylethene-based β-hairpin peptides as membranolytic antimicrobial and anticancer agents. J. Med. Chem. *61*, 10793–10813. https://doi.org/10.1021/acs.jmedchem.8b01428.

Bechinger, B. (1996). Towards membrane protein design: pH-sensitive topology of histidine-containing polypeptides. J. Mol. Biol. *263*, 768–775. https://doi.org/10.1006/JMBI.1996.0614.

Bechinger, B., Ruysschaert, J.-M., and Goormaghtigh, E. (1999). Membrane helix orientation from linear dichroism of infrared attenuated total reflection spectra. Biophys. J. *76*, 552–563. https://doi.org/10.1016/S0006-3495(99)77223-1.

Beharry, A.A., and Woolley, G.A. (2011). Azobenzene photoswitches for biomolecules. Chem. Soc. Rev. *40*, 4422–4437. https://doi.org/10.1039/c1cs15023e.

Blanco-Lomas, M., Samanta, S., Campos, P.J., Woolley, G.A., and Sampedro, D. (2012). Reversible photocontrol of peptide conformation with a rhodopsin-like photoswitch. J. Am. Chem. Soc. *134*, 6960–6963. https://doi.org/10.1021/ja301868p.

Bolen, D.W., and Rose, G.D. (2008). Structure and energetics of the hydrogen-bonded backbone in protein folding. Annu. Rev. Biochem. *77*, 339–362. https://doi.org/10.1146/annurev.biochem.77.061306.131357.

Brambillasca, S., Yabal, M., Makarow, M., and Borgese, N. (2006). Unassisted translocation of large polypeptide domains across phospholipid bilayers. J. Cell Biol. *175*, 767–777. https://doi.org/10.1083/jcb.200608101.

Bredenbeck, J., Helbing, J., Kumita, J.R., Woolley, G.A., and Hamm, P. (2005). α-helix formation in a photoswitchable peptide tracked from picoseconds to microseconds by time-resolved IR spectroscopy. Proc. Natl. Acad. Sci. U S A *102*, 2379–2384. https://doi.org/10.1073/pnas.0406948102.

Bürck, J., Wadhwani, P., Fanghänel, S., and Ulrich, A.S. (2016). Oriented circular dichroism: a method to characterize membrane-active peptides in oriented lipid bilayers. Acc. Chem. Res. *49*, 184–192. https://doi.org/10.1021/acs.accounts.5b00346.

Dave, N., Lórenz-Fonfría, V.A., Leblanc, G., and Padrós, E. (2008). FTIR spectroscopy of secondary-structure reorientation of melibiose permease modulated by substrate binding. Biophys. J. *94*, 3659–3670. https://doi.org/10.1529/biophysj.107.115550.

DeLange, F., Bovee-Geurts, P.H., Pistorius, A.M., Rothschild, K.J., and DeGrip, W.J. (1999). Probing intramolecular orientations in rhodopsin and metarhodopsin II by polarized infrared difference spectroscopy. Biochemistry *38*, 13200–13209. https://doi.org/10.1021/bi9909501.

Denschlag, R., Schreier, W.J., Rieff, B., Schrader, T.E., Koller, F.O., Moroder, L., Zinth, W., and Tavan, P. (2010). Relaxation time prediction for a light switchable peptide by molecular dynamics. Phys. Chem. Chem. Phys. *12*, 6204–6218. https://doi.org/10.1039/b921803c.

Earnest, T.N., Herzfeld, J., and Rothschild, K.J. (1990). Polarized Fourier transform infrared spectroscopy of bacteriorhodopsin. Transmembrane alpha helices are resistant to hydrogen/deuterium exchange. Biophys. J. *58*, 1539–1546. https://doi.org/10.1016/S0006-3495(90)82498-X.

Englander, S.W., Mayne, L., Kan, Z.-Y., and Hu, W. (2016). Protein folding—how and why: by hydrogen exchange, fragment separation, and mass spectrometry. Annu. Rev. Biophys. *45*, 135–152. https://doi.org/10.1146/annurev-biophys-062215-011121.

Esteban-Martín, S., Giménez, D., Fuertes, G., and Salgado, J. (2009). Orientational landscapes of peptides in membranes: prediction of 2H NMR couplings in a dynamic context. Biochemistry *48*, 11441–11448. https://doi.org/10.1021/bi901017y.

Flint, D.G., Kumita, J.R., Smart, O.S., and Woolley, G.A. (2002). Using an azobenzene cross-linker to either increase or decrease peptide helix content upon trans-to-cis photoisomerization. Chem. Biol. *9*, 391–397. https://doi.org/10.1016/S1074-5521(02)00109-6.

Fuertes, G., Giménez, D., Esteban-Martín, S., Sánchez-Muñoz, O.L., and Salgado, J. (2011). A lipocentric view of peptide-induced pores. Eur. Biophys. J. *40*, 399–415. https://doi.org/10.1007/s00249-011-0693-4.

Goormaghtigh, E., Cabiaux, V., and Ruysschaert, J.-M. (1994). Determination of soluble and membrane protein structure by fourier transform infrared spectroscopy. III. Secondary structures. Subcell. Biochem. *23*, 405–450. https://doi.org/10.1007/978-1-4615-1863-1_10.

Grdadolnik, J. (2003). Infrared difference spectroscopy: Part I. Interpretation of the difference spectrum. Vib. Spectrosc. *31*, 279–288. https://doi.org/10.1016/S0924-2031(03)00018-3.

Guha, S., Ghimire, J., Wu, E., and Wimley, W.C. (2019). Mechanistic landscape of membrane-permeabilizing peptides. Chem. Rev. *119*, 6040–6085. https://doi.org/10.1021/acs.chemrev.8b00520.

Hamm, P., Helbing, J., and Bredenbeck, J. (2008). Two-dimensional infrared spectroscopy of photoswitchable peptides. Annu. Rev. Phys. Chem. *59*, 291–317. https://doi.org/10.1146/annurev.physchem.59.032607.093757.

Hoersch, D., Roh, S.-H., Chiu, W., and Kortemme, T. (2013). Reprogramming an ATP-driven protein machine into a light-gated nanocage. Nat. Nanotechnol. *8*, 928–932. https://doi.org/10.1038/nnano.2013.242.

Hoorens, M.W.H., and Szymanski, W. (2018). Reversible, spatial and temporal control over protein activity using light. Trends Biochem. Sci. *43*, 567–575. https://doi.org/10.1016/J.TIBS.2018.05.004.

Hunt, J.F., Rath, P., Rothschild, K.J., and Engelman, D.M. (1997). Spontaneous, pH-dependent membrane insertion of a transbilayer alpha-helix. Biochemistry *36*, 15177–15192. https://doi.org/10.1021/bi970147b.

Ihalainen, J.A., Bredenbeck, J., Pfister, R., Helbing, J., Chi, L., van Stokkum, I.H.M., Woolley, G.A., and Hamm, P. (2007). Folding and unfolding of a photoswitchable peptide from picoseconds to microseconds. Proc. Natl. Acad. Sci. U S A *104*, 5383–5388. https://doi.org/10.1073/pnas.0607748104.

Kauppinen, J.K., Moffatt, D.J., Mantsch, H.H., Cameron, D.G., and Spectroscopy, R. (1981). Fourier self-deconvolution: a method for resolving intrinsically overlapped bands. Appl. Spectrosc. *35*, 271–276. https://doi.org/10.1366/0003702814732634.

Kim, G.C., Ahn, J.H., Oh, J.H., Nam, S., Hyun, S., Yu, J., and Lee, Y. (2018). Photoswitching of cell penetration of amphipathic peptides by control of α-helical conformation. Biomacromolecules *19*, 2863–2869. https://doi.org/10.1021/acs.biomac.8b00428.

Kneissl, S., Loveridge, E.J., Williams, C., Crump, M.P., and Allemann, R.K. (2008). Photocontrollable peptide-based switches target the anti-apoptotic protein Bcl-x L. ChemBioChem *9*, 3046–3054. https://doi.org/10.1002/cbic.200800502.

Kodati, V.R., and Lafleur, M. (1993). Comparison between orientational and conformational orders in fluid lipid bilayers. Biophys. J. *64*, 163–170. https://doi.org/10.1016/S0006-3495(93)81351-1.

Kottke, T., Lórenz-Fonfría, V.A., and Heberle, J. (2017). The grateful infrared: sequential protein structural changes resolved by infrared difference spectroscopy. J. Phys. Chem. B *121*, 335–350. https://doi.org/10.1021/acs.jpcb.6b09222.

Krimm, S., and Bandekar, J. (1986). Vibrational spectroscopy and conformation of peptides, polypeptides, and proteins. In Advances in Protein Chemistry (Academic Press), pp. 181–364. https://doi.org/10.1016/S0065-3233(08) 60528–8.

Kubelka, J. (2009). Time-resolved methods in biophysics. 9. Laser temperature-jump methods for investigating biomolecular dynamics. Photochem. Photobiol. Sci. *8*, 499–512. https://doi.org/10.1039/b819929a.

Kubelka, J., and Keiderling, T.A. (2001). Ab initio calculation of amide carbonyl stretch vibrational frequencies in solution with modified basis sets. 1. N -methyl acetamide. J. Phys. Chem. A *105*, 10922–10928. https://doi.org/10.1021/jp013203y.

Kučerka, N., Nieh, M.P., and Katsaras, J. (2011). Fluid phase lipid areas and bilayer thicknesses of commonly used phosphatidylcholines as a function of temperature. Biochim. Biophys. Acta *1808*, 2761–2771. https://doi.org/10.1016/j.bbamem.2011.07.022.

Kumita, J.R., Smart, O.S., and Woolley, G.A. (2000). Photo-control of helix content in a short peptide. Proc. Natl. Acad. Sci. *97*, 3803–3808. https://doi.org/10.1073/pnas.97.8.3803.

Lorenz-Fonfria, V.A. (2020). Infrared difference spectroscopy of proteins: from bands to bonds. Chem. Rev. *120*, 3466–3576. https://doi.org/10.1021/acs.chemrev.9b00449.

Lórenz-Fonfría, V.A., Bamann, C., Resler, T., Schlesinger, R., Bamberg, E., and Heberle, J. (2015). Temporal evolution of helix hydration in a light-gated ion channel correlates with ion conductance. Proc. Natl. Acad. Sci. U S A *112*, E5796–E5804. https://doi.org/10.1073/pnas.1511462112.

Lorenz-Fonfria, V.A., Granell, M., Leon, X., Leblanc, G., and Padros, E. (2009). In-plane and out-of-plane infrared difference spectroscopy unravels tilting of helices and structural changes in a membrane protein upon substrate binding. J. Am. Chem. Soc. *131*, 15094–15095. https://doi.org/10.1021/ja906324z.

Lórenz-Fonfría, V.A., and Padrós, E. (2004a). Curve-fitting of Fourier manipulated spectra comprising apodization, smoothing, derivation and deconvolution. Spectrochim. Acta A Mol. Biomol. Spectrosc. *60*, 2703–2710. https://doi.org/10.1016/j.saa.2004.01.008.

Lórenz-Fonfría, V.A., and Padrós, E. (2004b). Curve-fitting overlapped bands: quantification and improvement of curve-fitting robustness in the presence of errors in the model and in the data. Analyst *129*, 1243–1250. https://doi.org/10.1039/b406581f.

Lee, J., Lee, H., and Kim, C. (2020). Stimuli-responsive conformational transformation of antimicrobial peptides stapled with azobenzene unit. New J. Chem. *44*, 14777–14780.

Ludlam, C.F., Arkin, I.T., Liu, X.M., Rothman, M.S., Rath, P., Aimoto, S., Smith, S.O., Engelman, D.M., and Rothschild, K.J. (1996). Fourier transform infrared spectroscopy and site-directed isotope labeling as a probe of local secondary structure in the transmembrane domain of phospholamban. Biophys. J. *70*, 1728–1736. https://doi.org/10.1016/S0006-3495(96)79735-7.

Mantsch, H.H., and McElhaney, R.N. (1991). Phospholipid phase transitions in model and biological membranes as studied by infrared spectroscopy. Chem. Phys. Lipids *57*, 213–226. https://doi.org/10.1016/0009-3084(91)90077-O.

Marsh, D., Müller, M., and Schmitt, F.J. (2000). Orientation of the infrared transition moments for an alpha-helix. Biophys. J. *78*, 2499–2510. https://doi.org/10.1016/S0006-3495(00)76795-6.

Marsh, D., and Páli, T. (2001). Infrared dichroism from the X-ray structure of bacteriorhodopsin. Biophys. J. *80*, 305–312. https://doi.org/10.1016/S0006-3495(01)76015-8.

Mayo, D.J., Sahu, I.D., and Lorigan, G.A. (2018). Assessing topology and surface orientation of an antimicrobial peptide magainin 2 using mechanically aligned bilayers and electron paramagnetic resonance spectroscopy. Chem. Phys. Lipids *213*, 124–130. https://doi.org/10.1016/j.chemphyslip.2018.04.004.

Mutter, N.L., Volarić, J., Szymanski, W., Feringa, B.L., and Maglia, G. (2019). Reversible photocontrolled nanopore assembly. J. Am. Chem. Soc. *141*, 14356–14363. https://doi.org/10.1021/jacs.9b06998.

Nabedryk, E., and Breton, J. (1981). Orientation of intrinsic proteins in photosynthetic membranes. Polarized infrared spectroscopy of chloroplasts and chromatophores. Biochim. Biophys. Acta *635*, 515–524. https://doi.org/10.1016/0005-2728(81)90110-9.

Noguchi, T., and Sugiura, M. (2002). Flash-induced FTIR difference spectra of the water oxidizing complex in moderately hydrated photosystem II core films: effect of hydration extent on S-state transitions. Biochemistry *41*, 2322–2330. https://doi.org/10.1021/bi011954k.

Oh, K.-I., Fiorin, G., and Gai, F. (2015). How sensitive is the amide I vibration of the polypeptide backbone to electric fields? ChemPhysChem *16*, 3595–3598. https://doi.org/10.1002/cphc.201500777.

Park, E., and Rapoport, T.A. (2012). Mechanisms of sec61/SecY-mediated protein translocation across membranes. Annu. Rev. Biophys. *41*, 21–40. https://doi.org/10.1146/annurev-biophys-050511-102312.

Pfister, R., Ihalainen, J., Hamm, P., and Kolano, C. (2008). Synthesis, characterization and applicability of three isotope labeled azobenzene photoswitches. Org. Biomol. Chem. *6*, 3508. https://doi.org/10.1039/b804568b.

Pozhidaeva, N., Cormier, M.E., Chaudhari, A., and Woolley, G.A. (2004). Reversible photocontrol of peptide helix content: adjusting thermal stability of the cis state. Bioconjug. Chem. *15*, 1297–1303. https://doi.org/10.1021/bc049855h.

Rahmelow, K., Hübner, W., and Ackermann, T. (1998). Infrared absorbances of protein side chains. Anal. Biochem. *257*, 1–11. https://doi.org/10.1006/abio.1997.2502.

Roder, H., Maki, K., and Cheng, H. (2006). Early events in protein folding explored by rapid mixing methods. Chem. Rev. *106*, 1836–1861. https://doi.org/10.1021/cr040430y.

Rothschild, K.J., and Clark, N.A. (1979). Polarized infrared spectroscopy of oriented purple membrane. Biophys. J. *25*, 473–487. https://doi.org/10.1016/S0006-3495(79)85317-5.

Schuler, E.E., Nagarajan, S., and Dyer, R.B. (2016). Submillisecond dynamics of mastoparan X insertion into lipid membranes. J. Phys. Chem. Lett. *7*, 3365–3370. https://doi.org/10.1021/acs.jpclett.6b01512.

Snider, C., Jayasinghe, S., Hristova, K., and White, S.H. (2009). MPEx: a tool for exploring membrane proteins. Protein Sci. *18*, 2624–2628. https://doi.org/10.1002/pro.256.

Strandberg, E., Esteban-Martín, S., Ulrich, A.S., and Salgado, J. (2012). Hydrophobic mismatch of mobile transmembrane helices: merging theory and experiments. Biochim. Biophys. Acta *1818*, 1242–1249. https://doi.org/10.1016/j.bbamem.2012.01.023.

Strandberg, E., Horn, D., Reißer, S., Zerweck, J., Wadhwani, P., and Ulrich, A.S. (2016). 2H-NMR and MD simulations reveal membrane-bound conformation of magainin 2 and its synergy with PGLa. Biophys. J. *111*, 2149–2161. https://doi.org/10.1016/j.bpj.2016.10.012.

Szymański, W., Beierle, J.M., Kistemaker, H.A.V., Velema, W.A., and Feringa, B.L. (2013). Reversible photocontrol of biological systems by the incorporation of molecular photoswitches. Chem. Rev. *113*, 6114–6178. https://doi.org/10.1021/cr300179f.

Tamm, L.K., and Tatulian, S.A. (1997). Infrared spectroscopy of proteins and peptides in lipid bilayers. Q. Rev. Biophys. *30*, 365–429. https://doi.org/10.1016/S0006-3495(95)80150-5.

Tang, J., and Gai, F. (2008). Dissecting the membrane binding and insertion kinetics of a pHLIP peptide. Biochemistry *47*, 8250–8252. https://doi.org/10.1021/bi801103x.

Tsuboi, M. (1962). Infrared dichroism and molecular conformation of α-form poly-γ-benzyl-L-glutamate. J. Polym. Sci. *59*, 139–153. https://doi.org/10.1002/pol.1962.1205916712.

Tucker, M.J., Getahun, Z., Nanda, V., DeGrado, W.F., and Gai, F. (2004). A new method for determining the local environment and orientation of individual side chains of membrane-binding peptides. J. Am. Chem. Soc. *126*, 5078–5079. https://doi.org/10.1021/ja032015d.

Ulmschneider, J.P., Andersson, M., and Ulmschneider, M.B. (2011). Determining peptide partitioning properties via computer simulation. J. Membr. Biol. *239*, 15–26. https://doi.org/10.1007/s00232-010-9324-8.

Ulmschneider, J.P., and Ulmschneider, M.B. (2018). Molecular dynamics simulations are redefining our view of peptides interacting with biological membranes. Acc. Chem. Res. *51*, 1106–1116. https://doi.org/10.1021/acs.accounts.7b00613.

Ulmschneider, M.B., Doux, J.P.F., Killian, J.A., Smith, J.C., and Ulmschneider, J.P. (2010). Mechanism and kinetics of peptide partitioning into membranes from all-atom simulations of thermostable peptides. J. Am. Chem. Soc. *132*, 3452–3460. https://doi.org/10.1021/ja909347x.

Venyaminov, S.Yu, and Kalnin, N.N. (1990). Quantitative IR spectrophotometry of peptide compounds in water (H_2O) solutions. II. Amide absorption bands of polypeptides and fibrous proteins in α-, β-, and random coil conformations. Biopolymers *30*, 1259–1271. https://doi.org/10.1002/bip.360301310.

Vogt, T.C., and Bechinger, B. (1999). The interactions of histidine-containing amphipathic helical peptide antibiotics with lipid bilayers. The effects of charges and pH. J. Biol. Chem. *274*, 29115–29121. https://doi.org/10.1074/jbc.274.41.29115.

Walsh, S.T.R.R., Cheng, R.P., Wright, W.W., Alonso, D.O.V., Daggett, V., Jane, M., Degrado, W.F., Vanderkooi, J.M., and Grado, W.F.D.E. (2003). The hydration of amides in helices; a comprehensive picture from molecular dynamics, IR, and NMR. Protein Sci. *12*, 520–531. https://doi.org/10.1110/ps.0223003.

Whiles, J.A., Brasseur, R., Glover, K.J., Melacini, G., Komives, E.A., and Vold, R.R. (2001). Orientation and effects of mastoparan X on phospholipid bicelles. Biophys. J. *80*, 280–293. https://doi.org/10.1016/S0006-3495(01)76013-4.

White, S.H., and Wimley, W.C. (1999). Membrane protein folding and stability: physical principles. Annu. Rev. Biophys. Biomol. Struct. *28*, 319–365. https://doi.org/10.1146/annurev.biophys.28.1.319.

Wimley, W.C., Creamer, T.P., and White, S.H. (1996). Solvation energies of amino acid side chains and backbone in a family of host-guest pentapeptides. Biochemistry *35*, 5109–5124. https://doi.org/10.1021/bi9600153.

Wimley, W.C., and White, S.H. (1996). Experimentally determined hydrophobicity scale for proteins at membrane interfaces. Nat. Struct. Biol. *3*, 842–848. https://doi.org/10.1038/nsb1096-842.

Woolley, G.A. (2005). Photocontrolling peptide alpha helices. Acc. Chem. Res. *38*, 486–493. https://doi.org/10.1021/ar040091v.

Wu, Y., Huang, H.W., and Olah, G.A. (1990). Method of oriented circular dichroism. Biophys. J. *57*, 797–806. https://doi.org/10.1016/S0006-3495(90)82599-6.

Wyatt, L.C., Moshnikova, A., Crawford, T., Engelman, D.M., Andreev, O.A., and Reshetnyak, Y.K. (2018). Peptides of pHLIP family for targeted intracellular and extracellular delivery of cargo molecules to tumors. Proc. Natl. Acad. Sci. U S A *115*, E2811–E2818. https://doi.org/10.1073/pnas.1715350115.

Yeoh, Y.Q., Yu, J., Polyak, S.W., Horsley, J.R., and Abell, A.D. (2018). Photopharmacological control of cyclic antimicrobial peptides. ChemBioChem *19*, 2591–2597. https://doi.org/10.1002/cbic.201800618.

Zhang, Y., Lewis, R.N.A.H., Henry, G.D., Sykes, B.D., Hodges, R.S., and McElhaney, R.N. (1995). Peptide models of helical hydrophobic transmembrane segments of membrane proteins. 1. Studies of the conformation, intrabilayer orientation, and amide hydrogen exchangeability of Ac-K_2-$(LA)_{12}$-K_2. Biochemistry *34*, 2348–2361. https://doi.org/10.1021/bi00007a031.

STAR★METHODS

KEY RESOURCES TABLE

REAGENT or RESOURCE	SOURCE	IDENTIFIER
Chemicals, peptides, and recombinant proteins		
KCALP	This paper	N/A
KCALP-azo	This paper	N/A
KALP	Genscript	RRID:SCR_002891
ThioAzo	This paper	N/A
BCA	(Pozhidaeva et al., 2004)	N/A
LAH_4	(Vogt and Bechinger, 1999)	N/A
POPC	Avanti Polar Lipids	850457
Software and algorithms		
Matlab R2020a	https://www.mathworks.com	RRID: SCR_001622
Origin 9.6 (2019)	https://www.originlab.com	RRID: SCR_014212
FourierDataProcessing v0.1	Victor Lorenz-Fonfria	https://es.mathworks.com/matlabcentral/fileexchange/92573-fourierdataprocessing
Other		
FTIR spectrometer	Bruker	Vertex 80
FTIR spectrometer	ThermoFisher Scientific	Nicolet 5700
CD spectrometer	Jasco	J-810
UV-Vis spectrometer	OceanOptics	Flame-S-UV-Vis
BaF_2 windows	Korth Krystalle	N/A
MicromATR with 3 reflections Si Duradisk	Czitek	N/A
LED Driver	Thorlabs	LEDD1B
Motorized rotational stage	Thorlabs	PRM1/MZ8
BaF_2 holographic wire grid polarizer	Thorlabs	WP25H-B
Automated Microwave Peptide Synthesizer	CEM	Liberty Blue
Semi-preparative HPLC	Waters	Delta Prep 4000
Analytical HPLC	Waters	1525
MASS spectrometer	Bruker Daltonics	micrOTOF-Q
NMR spectrometer	Bruker	AVANCE III HD (300 MHz)

RESOURCE AVAILABILITY

Lead contact

Further information and requests for resources should be directed to and will be fulfilled by the lead contact: Victor A. Lorenz-Fonfria (victor.lorenz@uv.es).

Materials availability

There are restrictions to the availability of the peptide KCALP-azo to third parties due to its cost and its quantity synthetized.

Data and code availability

Original data for Figures 2, 3, 4, 5 and 6 in the paper are available at Mendeley Data [https://doi.org/10.17632/d5tbfypwcg.1]. Part of the Matlab programs/scripts used to analyze data in the paper are available at Matlab File Exchange (https://es.mathworks.com/matlabcentral/fileexchange/92573-fourierdataprocessing), and the rest is available upon reasonable request.

METHODS DETAILS

Peptide synthesis and purification

KALP, with sequence Ac-GKKLLAALLAALLAALLAALLKKA-NH_2, was purchased from Genscript. The peptide purity was ~95% (determined by HPLC), and trifluoroacetic acid (TFA) was exchanged to chloride as a counterion. KCALP (see Figure 1 for its sequence), and LAH_4, with sequence KKALLALALHHLAHLALHLALALKKA-NH_2 (Vogt and Bechinger, 1999), were prepared by a stepwise micro-wave assisted solid-phase peptide synthesis on a Liberty Blue synthesizer using the standard Fmoc/tBu strategy. Both peptides were constructed on a Rink Amide MBHA resin using a 5-fold molar excess of Fmoc-protected amino acids for chain elongation, acetic anhydride/pyridine 1/2 (v/v) for N-terminus acetylation, and TFA/thioanisole/1,2-ethanedithiol/anisole 90/5/3/2 (v/v/v/v) for final cleavage from the resin and removal of side chain protecting groups. Crude peptides were purified by semi-preparative RP-HPLC on a Phenomenex Luna C8(2) column (10 μm, 250 mm x 21.2 mm) using an acetonitrile/water gradient in 0.1% TFA. After lyophilization, the TFA counterions, which hamper physicochemical characterization by FTIR spectroscopy, were exchanged to chloride using a strong base anion exchange resin (AMBERLITE™ IRA402 Cl). High-resolution electrospray-ionization mass spectra (HRMS-ESI+) confirmed the identity of the peptides. KCALP: m/z for $C_{115}H_{214}N_{29}O_{25}S_2$ $[M+3H]^{3+}$ calculated 821.8597, found 822.1969 (Figure S13C); LAH_4: m/z for $C_{132}H_{233}N_{39}O_{26}$ $[M+4H]^{4+}$ calculated 695.2022, found 695.4522 (Figure S14C). HRMS-ESI+ was recorded in positive ion mode on a micrOTOF-Q spectrometer (Bruker), with sodium formate as an external reference. The purity of the peptides (>95%) was checked by analytical HPLC on a Phenomenex Luna C8(2) column (5 μm, 250 mm x 4.6 mm), as explained in Figure S13B (for KCALP) and Figure S14B (for LAH_4).

Synthesis of KCALP-azo, BCA and ThioAzo

KCALP (16 mg, 6.5 mmol) and the reducing agent tris(carboxyethyl)phosphine (7.45 mg, 26 mmol) were mixed and incubated overnight under an inert atmosphere of argon in a mixture of trifluoroethanol (TFE)/100 mM ammonium bicarbonate buffer (1/1 v/v, 10.2 mL, pH 8.5). A solution of BCA cross-linker (9.46 mg, 26 mmol) in dimethyl sulfoxide (2.6 mL) was added, and the mixture was stirred at 40°C in the dark until completion of the reaction (monitored by MALDI-TOF mass spectrometry). The cross-linked peptide was purified by RP-HPLC and characterized by HRMS-ESI+: m/z for $C_{131}H_{226}N_{33}O_{27}S_2$ $[M+3H]^{3+}$ calculated 919.2250, found 919.5601 (Figure S15C). The TFA counterions were exchanged for chloride as described for KCALP, and the purity of the product (>95%) was checked by analytical HPLC on a Phenomenex Luna C8(2), as shown in Figure S15B. BCA (4,4′-bis(chloroacetamide)azobenzene) was synthesized according to literature, with spectral properties matching previously reported values (Pozhidaeva et al., 2004). ThioAzo ((*E*)-N,N′-(diazene-1,2-diylbis(4,1-phenylene))bis(2-((2-hydroxyethyl)thio)acetamide) was synthesized as described above for KCALP-azo, except that 2-mercaptoethanol was used for the reaction with BCA instead of KCALP. The pure product was characterized by HRMS-ESI+ (Figure S18) as well as by ^{1}H and ^{13}C NMR (Figures S16 and S17), the latter recorded on a Bruker AVANCE III HD spectrometer (300 MHz).

Peptide reconstitution in POPC membranes

Lyophilized peptides (KALP, KCALP, KCALP-azo and LAH_4) were weighted, dissolved in TFE and mixed with in the appropriate amount of the POPC lipid (Avanti) in chloroform/methanol 2/1 (v/v), to a target lipid/peptide ratio of 20 (mol/mol), and dried in a N_2 atmosphere (followed by 2 hours of vacuum). Then, buffer was added, and the mixture was vigorously vortexed to form large multilamellar vesicles (LMV), washed 3 times by ultracentrifugation (50,000 RPM for 50 minutes), and finally resuspended in the appropriate volume of buffer (2 mM sodium phosphate at pH 7). Likewise, we prepared LMVs containing the ThioAzo compound alone, as well as LMVs containing equimolar amounts of KCALP and ThioAzo.

Preparation and characterization of oriented films

We dried KCALP or KCALP-azo reconstituted in POPC vesicles (10-15 μL) at ambient humidity over BaF_2 windows, forming films of ~6-8 mm diameter. For ATR experiments, ~2-4 μL of KALP, KCALP, KCALP-azo or LAH_4, reconstituted in POPC vesicles, were dried on a silicon crystal with 3 total reflections (DuraDisk, Czitek). These films were hydrated by the atmosphere created by drops of water/glycerol (see Figure 3A, left) following previous work (Noguchi and Sugiura, 2002). We estimated the final number of water molecules per peptide as described in Figure S4. This ratio was ~950 in hydrated films used for unpolarized light-induced FTIR experiments (Figure 4) and for polarized light-induced FTIR experiments by ATR

(Figure 5A), and ~450 for the rest of measurements (Figures 3 and Figure 5B). Both hydration levels provided similar results (see Figure S5).

FTIR measurements

Unpolarized FTIR absorption spectra were collected at 2 cm^{-1} spectral resolution, and light-induced unpolarized spectra at 4 cm^{-1} resolution, using either a Vertex 80v or a Vertex 80 FTIR spectrometer (Bruker) equipped with a photovoltaic MCT detector. Polarized absorption spectra were collected at 4 cm^{-1} resolution on a Nicolet 5700 (ThermoFisher) FTIR spectrometer equipped with a photoconductive MCT, using a BaF_2 holographic wire grid polarizer (Thorlabs) mounted on a motorized rotational stage (Thorlabs, PRM1/MZ8). Polarized light-induced FTIR difference spectra were measured similarly, but on a Vertex 80 FTIR spectrometer. Illumination during transmission experiments was achieved using @365 nm and @447 nm LEDs, with power densities at the sample of ~400 mW/cm^2 and ~200 mW/cm^2, as measured with a power-meter (Thorlabs, PM160T). For ATR experiments the samples were illuminated from the top, with @365 nm and @455 nm LEDS coupled to optical fibers, with power densities at the sample of ~20 mW/cm^2. All the experiments were conducted at room temperature (~25°C).

UV-Vis measurements

UV-Vis absorption spectra of the pure *cis* and *trans* isomers of KCALP-azo were recorded by a Waters 2998 photodiode array detector built into the analytical HPLC equipment (Figure S9C). This allowed to determine the percentage of each isomer in solution (1/1 (v/v) acetonitrile/water +0.1% TFA), as described in Figure S9. UV-Vis absorption spectra of hydrated films of KCALP-azo in POPC were measured in a home-made optical setup using an array detector (Flame-S-UV-Vis, OceanOptics). The absorption spectra of KCALP-azo were corrected from scattering using an absorption spectrum of a KCALP film as a blank.

OCD measurements

A hydrated film of lipid reconstituted KCALP-azo on a BaF_2 window (covered by a second window), was placed in a rotating holder, perpendicular to the circularly polarized beam. A circular iris of 4 mm diameter was used to block part of the rectangular light beam, ensuring that all the detected light went through the film. Absorption and CD spectra were simultaneously collected from 600 to 190 nm in 0.5 nm steps, at 100 nm/min and with a 4 nm slit, using a Jasco J-810 spectropolarimeter. A baseline recorded with the sample compartment empty was subtracted from the data to minimize potential linear dichroism contributions to the CD spectrum, a CD spectrum was recorded after rotating the sample 30°, a process repeated 12 times until the window made a full turn (Wu et al., 1990). Illumination to photoisomerize the azobenzene was performed by turning on for 2 s LEDs with λ_{max} at 365 nm (~400 mW/cm^2) and 447 nm (~200 mW/cm^2).

QUANTIFICATION AND STATISTICAL ANALYSIS

Spectral analysis

FSD and band-fitting of FSD spectra were performed using previously described scripts running in MATLAB (Lórenz-Fonfría and Padrós, 2004a, 2004b), implemented in the Matlab App "FourierDataProcessing.mlappinstall", available at the Matlab File Exchange (https://es.mathworks.com/matlabcentral/fileexchange/92573-fourierdataprocessing). For FSD, we used a narrowing factor (k) of 2.0 and a Lorentzian width (γ_L) of 18 cm^{-1}, except in the analysis of Figures 4D and 4E (k = 2.0 and γ_L = 12 cm^{-1}) and in the amide A range in Figure 3D (k = 2.0 and γ_L = 50 cm^{-1}). We fitted FSD spectra using FSD-modified Voigtian bands, using a method that takes into account bandshape changes introduced by FSD (Lórenz-Fonfría and Padrós, 2004a, 2004b), implemented in the home-made Matlab programs "cffsdv.m" and "cffsdv_diff.m".

Determination of helical tilts

We applied Equation 1 to estimate S_β, using randomly generated values for α, n_2, S_{ms}, S_ϕ and R, from a uniform distribution accounting for their uncertainty. For the tilt angle of the sample window, α, we considered a uniform distribution from 48° to 52°. For n_2 we used a uniform distribution from 1.45 to 1.55 for dry films, and from 1.35 to 1.45 for hydrated films. Regarding S_ϕ, we assumed values of ϕ to follow a uniform distribution from 27° and 34° for the amide A vibration, from 38° and 41.5° for the amide I, and from 68° and 76° for the amide II (Marsh et al., 2000; Marsh and Páli, 2001; Tsuboi, 1962). The value of S_{ms} in hydrated films was estimated to be 0.88 ± 0.03 by comparing the order parameter for the ν_sCH vibration determined by polarized FTIR experiments, −0.145 ± 0.005, with the one deduced using a published correlation between the order parameter and the ν_sCH frequency (Kodati and Lafleur, 1993): −0.170 ± 0.005 for a 2853.45 ± 0.05 cm^{-1} ν_sCH frequency. We assumed

that the same value for S_{ms} applies to the dry films. Finally, we generously assumed the experimental value of R to have an error of $\pm$ 0.02. To obtain probability distributions for S_β, we generated 10^6 random samples, binning the results, and normalizing the area to 1. A global estimate was obtained by multiplying distributions for S_β obtained from the dichroic ratio of the amide A, I and II vibrations, normalizing the result to 1. To estimate the average helical tilt, $\langle\beta\rangle$, from the global distribution of S_β, we used the approximation $S_\beta \approx \left(3cos^2\langle\beta\rangle - 1\right)/2$. The validation of this approximation is presented in Figure S7. All these calculations were automatized using a script running in Matlab.